Title
TESTS OF GAS SAMPLING ELECTROMAGNETIC SHOWER CALORIMETER

Author
Barbaro-Galtieri, A.

Publication Date
1982-11-01

LBL-15030
Preprint

Lawrence Berkeley Laboratory
UNIVERSITY OF CALIFORNIA

Physics, Computer Science & Mathematics Division

Submitted to Nuclear Instruments and Methods

TESTS OF GAS SAMPLING ELECTROMAGNETIC SHOWER CALORIMETER

A. Barbaro-Galtieri, W. Carithers, C. Day,
K.J. Johnson, W.A. Wenzel, and H. Videau

November 1982

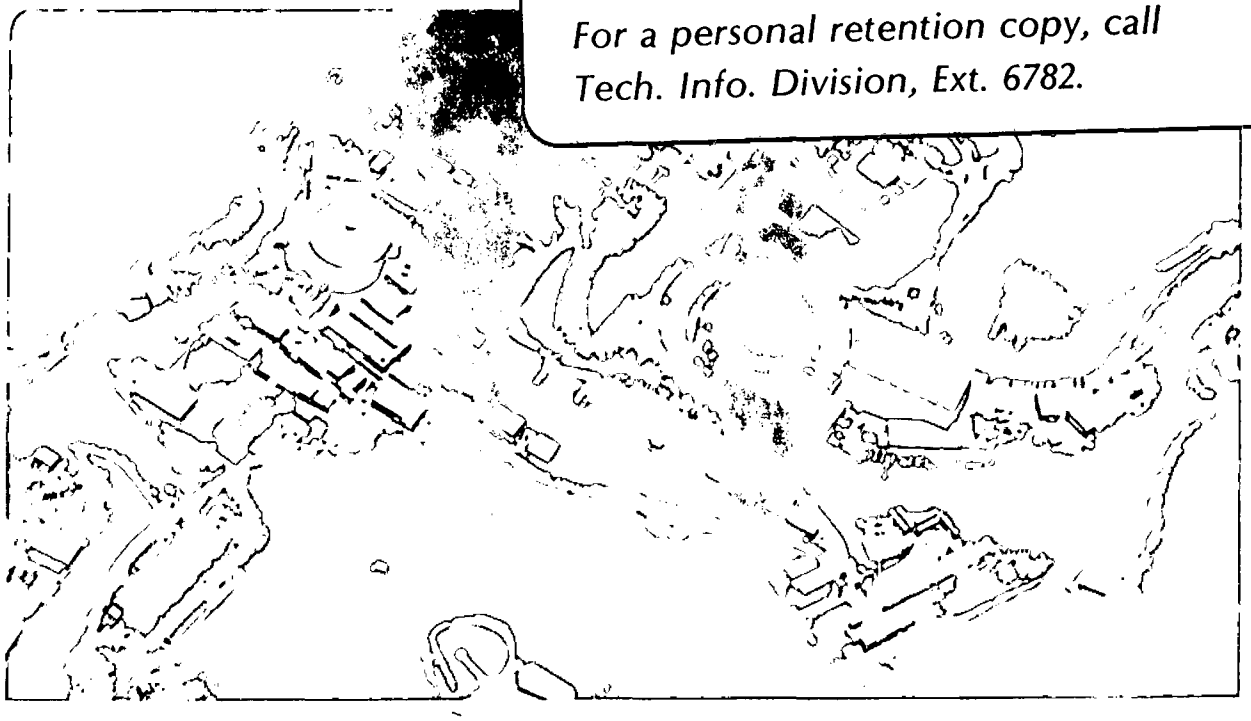

Prepared for the U.S. Department of Energy under Contract DE-AC03-76SF00098

DISCLAIMER

LBL-15030

Tests of Gas Sampling Electromagnetic Shower Calorimeter

A. Barbaro-Galtieri, W. Carithers, C. Day, K.J. Johnson, and W.A. Wenzel,
Lawrence Berkeley Laboratory, University of California, Berkeley, California 94720
and
H. Videau, Lawrence Berkeley Laboratory and Ecole Polytechnique, Palaiseau, France

ABSTRACT

An electromagnetic shower gas-sampling calorimeter has been tested in both Geiger and proportional discharge modes for incident electron energies in the range 0.125-16 GeV. The 0.2 radiation length-thick layers were lead-fiberglass laminates with cathode strips normal to the sense wires. The 5 x 10 mm^2 Geiger cells were formed with uniformly spaced nylon fibers perpendicular to the wires. Proportional mode measurements were carried out in the pressure range 1-10 atmospheres. A Monte Carlo simulation is in good agreement with measured shower characteristics and has been used to predict the behavior for oblique angles of incidence and for various Geiger cell dimensions.

Supported by the Director, Office of Energy Research, Office of Basic Energy Sciences, of the U.S. Department of Energy under Contract No. DE-AC03-76SF00098 and by Centre National de la Recherche Scientifique, France.

I. INTRODUCTION

Sampling calorimeters using gas as the sensitive medium offer some special advantages over those with dense (e.g. scintillator or liquid argon) sampling layers. Such advantages may include excellent spatial resolution, low noise, and various operational features.

For all sampling calorimeters the energy resolution is limited by fluctuations in the number of shower secondaries in the sensitive gap. For gas detectors measuring ionization, there are two additional major sources of fluctuation: the oblique low energy shower particle tracks and the high energy component of the energy loss distribution (Landau fluctuations). These effects degrade the energy resolution expected from shower statistics by a factor of approximately two.

The best energy resolution would be obtained by simply counting shower secondaries. A first attempt in this direction is the design used by Federici et al.[1], in which individual cells consisting of long flash tubes of small cross sectional area are discharged by the passage of shower secondaries. The shower energy is measured by counting the number of discharged tubes. Fluctuations are limited because each discharge is independent of both initial ionization and longitudinal track obliquity. The relatively large area of each tube produces large saturation effects, so that the usefulness of this technique is limited to relatively low energies or low density applications.

The development program reported here was carried out in spring

1979 for the design of the electromagnetic hexagonal calorimeter for the PEP-4 (Time Projection Chamber) facility at PEP. The requirements for this calorimeter are good signal-to-noise ratio with both spatial and energy resolutions adequate to resolve particles within jets and to measure low energy secondaries. It should complement the particle identification capability of the TPC by providing some electron-pion separation. Constraints include limited space and budget.

We have tested a sampling calorimeter module using gas with amplifying wires operated in either the Geiger or proportional mode. Induced cathode signals in each gap localize the discharges along the wires. Because the Geiger discharge is independent of initial ionization, the Landau fluctuations are suppressed and the energy resolution may be improved relative to that for the same calorimeter operated in proportional mode. We expect operation in the Geiger mode to be stable, providing large signals and related simplification of the electronics. The Geiger mode design is expected to suffer from saturation at high energies, however, giving a signal response that is nonlinear with energy.

In Section II the principles of Geiger mode operation and some bench tests are discussed. Section III describes the experimental apparatus and test set-up in the e-π beam. Section IV discusses a Monte Carlo simulation of the calorimeter performance. Section V presents and discusses the results of the beam tests. Our conclusions are in Section VI.

II. BENCH TESTS OF GEIGER MODE DISCHARGE

A. Principles of Geiger Mode Operation

Operation in the Geiger region requires a quenching gas with an appropriate photoionization cross section. One or more electrons from the primary ionization drift into the high field region surrounding the anode wire. Multiplication proceeds by ionizing collisions which generate an avalanche. Radial development of the avalanche stops when the space charge is sufficient to reduce the electric field below threshold (self-quenching streamer limit). However, ultra-violet photons photoionize the quenching gas, producing electrons which initiate new avalanches further along the anode wire. The discharge spreads along the entire wire, which is then dead until the positive ions are cleared. The small mobilities of these ions cause appreciable dead time, typically $\sim 10^{-4}$ sec.

To minimize the effects of dead time and saturation, and to provide good spatial resolution along the anode wire, our calorimeter design uses artificially interrupted Geiger dicharges 10 mm in length. That is, each wire is divided into many independent electrically-ganged Geiger counters. For our application this increases the capacity of the calorimeter to record tracks by more than two orders of magnitude above what would be possible without segmentation. Both the track pile-up and the dead time problems are thereby reduced.

There are several ways to interrupt the Geiger streamer. One is

to increase the anode wire diameter locally with blobs[2]. We have chosen instead to place thin filaments of nylon across the wires. In the design of a large area calorimeter these filaments will serve also to support the wires. The filaments are extremely efficient in stopping the Geiger streamers, but are found to produce inefficient or dead regions, presumably because charge which builds up on the dielectric collects ionization without multiplication.

Various gas mixtures could be used in our application. We have followed the early work of Charpak and Sauli[3], who showed that ordinary PWC planes can be operated reliably in the Geiger region using argon with a few percent ethyl bromide (C_2H_5Br). For large concentrations of ethyl bromide the counting efficiency is reduced dramatically. At very low concentrations the ultra-violet photon mean free path increases to the extent that discharges on neighboring anode wires are initiated.

Because the avalanche proceeds to a space charge limit, and the Geiger discharge is made of numerous avalanches, the inherent pulse height uniformity of the Geiger counter is very good. In the segmented calorimeter design a number of factors degrade this uniformity, but it is good enough so that the number of contributing cells can be counted by measuring the total pulse height. This is investigated below in some detail.

B. Single Plane Bench Tests of Geiger Mode

Before constructing a calorimeter we have performed a number of

tests on single plane configurations. Signals were measured using a Tektronics 475 oscilloscope or a LeCroy QVT pulse height analyzer. Particle sources included Fe^{55} (5.9 keV-γ), Ru^{106} (3.5 MeV-β) and cosmic rays. Two typical wire plane configurations are shown in Figure 1.

The most dramatic result of our tests was the uniformity in pulse height. Figure 2 shows the resolution for a 200 mm-long unsegmented anode wire. Figure 3 shows the effect of segmenting the wire. A diagonal nylon fiber (Figure 1) defines a set of wires whose effective lengths vary with position. The duration of the measured pulse is proportional to wire length, and the pulse height is approximately constant (Figure 3).

For the uniformly segmented configuration shown in Figure 1 each cell contributes a quantum of charge that is remarkably constant. For a cell size 5 mm x 10 mm, Figure 4a shows the pulse height spectrum obtained by connecting all anode wires together and illuminating the plane with a diffuse beta source. The main peak shows the discharge of a single cell. A track crossing cell boundaries discharges more than one cell. In Figure 4b the data for a very long run are displayed on a logarithmic scale. Ten peaks are clearly resolved. The maximum observed multiplicity is limited by counting statistics.

A charged particle detection efficiency ε less than unity implies a degradation of calorimeter energy resolution, which depends on the number of tracks, by a factor $\varepsilon^{-\frac{1}{2}}$. With cosmic ray triggers the average efficiency of the wire plane under typical operating conditions

(3-4 percent ethyl bromide) was measured to be 0.8. With the chamber geometry used here at concentrations of approximately 6 percent the efficiency deteriorated significantly. At 2 percent, the parasitic discharge of neighboring cells increased significantly.

III. BEAM TESTS OF CALORIMETER MODULE

A. Calorimeter Module Construction

To test the response of the Geiger mode design to electromagnetic showers, a calorimeter module was constructed of 305 x 305 mm^2, 0.21 radiation length-thick aluminum-fiberglass-lead laminates separated by 5 mm-thick gas gaps (Figure 5). Details of the laminate and gap are shown in Figure 6. Each aluminum surface was etched with twelve 15 mm-wide strips which served as cathodes. The gold-plated tungsten anode wires, 0.02 mm in diameter, spaced every 5mm, were orthogonal to the strips. In each gap these were connected in threes to provide eleven signal elements. Nylon monofilaments 0.15 mm in diameter were stretched across the wires at 10 mm intervals to define a matrix of 5x10 mm^2 cells. The fiberglass (G10) had two important functions. It insulated the cathode strips and provided laminate strength and rigidity.

The total calorimeter was 15.2 radiation lengths thick. The 72 gas-laminate layers were segmented in depth into four electrically independent sub-modules of 18 layers each. Within a module, signals from

the anode wires (cathode strips) were paralleled in depth to form 35 (48) channels in total. The channel configurations were chosen to study various characteristics of the calorimeter including total anode and cathode signals, development of the showers in depth and transverse to the beam and the ratio of signals on downstream and upstream cathodes.

The calorimeter was installed in a steel cylinder which could be operated from 0 to 10 atmospheres pressure. For Geiger mode operation the pressure vessel was first evacuated. Then a measured volume of liquid ethyl bromide was injected. Finally the vessel was filled with argon gas to atmospheric pressure. The vessel was then sealed off. Tests were carried out with ethyl bromide (molar) concentrations of 3 and 4 percent.

B. Electronics

Normal operation with an anode voltage of ~1 kV gave signals large enough that only passive components were needed to drive the Lecroy 2249A analogue-to-digital (ADC) converters. A peaking circuit (Figure 7) for each channel was matched directly to the 50-ohm line. The transformer served to avoid possible ground loops and to select polarity (opposite for anode and cathode signals). The turns ratio and the shimming capacitors were chosen to provide critically damped pulses with 1.88 microsecond peaking times.

The electronic calibration of all channels was accomplished by

discharging a calibration capacitor at the primary of each transformer. The calibration charges were supplied from a ballast capacitor charged from a 12 bit digital to analogue converter (DAC) and discharged through a mercury relay into a low impedance load. The calibration voltage range (0.0125-10 volts) provided 1-800 counts (0.25-200 picocoulombs) in the ADC's. For each wire channel an independently measured factor in the range 1.02-1.18 corrected for signal charge lost on the high voltage coupling capacitor.

In order to handle the large dynamic range required for electron energies in the 0.125-16 GeV range, two sampling-gate widths, 50 and 150 ns, were used for the ADC's. The calibration procedure automatically normalized the two sets of data to establish a consistent scale in ADC counts vs charge. For convenience we define the collected charge Q in terms of the ADC counts obtained with the wider gate.

Data were collected using a Hewlett Packard Model 2100 computer. In addition to reading the ADC's the computer monitored calorimeter high voltage, current and pressure. It also controlled the calibration sequence and provided digital amplitudes to the DAC.

C. Beam

The calorimeter was tested in the SLAC C-beam[4] using electrons and pions in the momentum range 0.125-16 GeV/c. The beam was collimated to a diameter of $\sim$10 mm using an aperture stop and two halo scintillation counters. It entered the calorimeter vessel though the end flange via

a 25 mm diameter hole covered by a thin aluminum window. Particles were selected with a scintillation counter, and electrons were tagged with a gas Cherenkov counter. A pile-up circuit prevented data-taking if there was more than one beam particle per accelerator burst.

D. Proportional Mode Tests

The same basic calorimeter was used to test proportional mode operation. These changes were involved:

1. There were no nylon monofilaments in the gas gaps.
2. Preamplifiers were added at the calorimeter with amplifiers nearby. These provided peaking and matching to the ADC's.
3. The gas was a mixture of 90 percent argon and 10 percent methane in the pressure range 1-10 atmospheres.
4. The number of wire (strip) channels was 27(47).

IV. MONTE CARLO SIMULATION OF THE CALORIMETER PERFORMANCE

A. Procedure

A detailed simulation of the calorimeter performance was developed to disentangle the various factors contributing to the resolution, to examine the behavior at incident angles that we did not try experimentally and to infer the best cell size for operation.

We have simulated both proportional and Geiger mode operation using the program EGS[5] as a generator. The exact material and geometry of the test module have been used, including the layers of fiberglass (G10) and aluminum that support the lead. To save computer time in particle tracking we have used the standard version of the program with a lower energy limit of 1.5 MeV for the electrons and 0.1 MeV for the photons. Comparisons with the experimental measurements indicate that the limit on the electron energy is large enough to introduce some inaccurracies which will be discussed below.

Another approximation in the procedure, also introduced to save time, is to neglect the effect of the gas gaps on the development of the shower. In the first step of the simulation, therefore, the gaps are treated as empty, and a file is generated containing the parameters of all particles entering the gaps. The second step of the simulation deals with what is happening in the gaps: the charged tracks are followed in the one-atmosphere gas using small steps. Multiple scattering is generated according to Moliere's formula, and the energy is collected following a procedure similar to that described by Ispirian[6]. The accuracy of this procedure has been verified by comparison with dE/dx measurements[7].

To calculate the energy deposited in the gap by energetic delta rays we assume that the maximum delta ray path length in any gap is of the order of the gap width. This procedure provides an equivalent maximum energy loss cut of $\sim$30 keV, much larger than the most probable electron energy loss of 1.5 keV. These delta rays, therefore, give a

very asymmetrical energy loss distribution. To take into account the fluctuations in the signal collection process, we smear the energy deposited in each gap by an additional twenty percent.

For the Geiger mode simulation we count the number of discharged cells. Each plane of wires and nylon fibers is simulated as a grid with an origin randomly distributed (modulo one cell). For each cell the single particle counting efficiency function ε is assumed to have a one dimensional dependence on position as follows: $\varepsilon=0$ at each nylon fiber, rising linearly in 1 mm to 0.8, and retaining this value across the cell to within 1 mm of the other fiber boundary. This gives $\langle\varepsilon\rangle=0.72$ for the 10 mm-long cell, consistent with the measurements shown in Table I and discussed below.

B. Contributions to Energy Resolution

Using the simulation procedure discussed above we have studied the various factors contributing to the measured calorimeter energy resolution.

1. Number of track segments

The number and distribution of track segments has been studied for various electron energies and sampling thicknesses. In all cases the distributions were found to be Gaussian. Figures 8 and 9 show that for our sampling thickness (t=0.2 r.l.) the linearity of number of tracks with energy is excellent and that the rms energy resolution with track counting would be

$$\sigma_E/E = \alpha\ [E\ (\mathrm{GeV})]^{-\frac{1}{2}}$$

with $\alpha = 0.05$. For the 15.2 r.l. test calorimeter the loss of shower information out the back degrades the resolution for energies above a few GeV. This is shown in Figure 9, where the simulations for a 21 r.l.-thick calorimeter are presented for comparison.

As a check on the procedure, we have compared simulations at 0.25 GeV for sampling thicknesses t=0.1, 0.2 and 0.4 radiation lengths. Not only does the number of tracks show the expected inverse proportionality with t but the energy resolution, within the accuracy of our simulation, verifies the familiar relation for sampling calorimeters

$$\sigma_E/E = K\,[\,t\ (\text{r.l.})/E\ (\text{GeV})]^{\frac{1}{2}}$$

where we find K=0.11.

Except for the absolute value of K, therefore, the energy resolution behaves as if each track segment is randomly generated. It is obvious, however, that there are correlations among the segments. At 1 GeV, for example, the number of tracks is 177 for t=0.2 r.l. Without correlations we would expect to find $K=[177(0.2)]^{-\frac{1}{2}}=0.17$, whereas the simulated value given above is only 2/3 as large.

2. Track Obliquity

Unlike the number of tracks, the total simulated path length of tracks in the gaps grows slightly faster than linearly with energy. There are two possible reasons why this could be spurious. First, the distributions are asymmetric, with tails on the large path length side. These make it difficult to determine the mean values and widths.

Second, there is evidence that the average path lengths are artificially reduced in the standard EGS program because the cut-off value (1.5 MeV) for the minimum electron energy is too high. At low energies the path length energy resolution (Figure 9) also deviates from the expected $E^{-\frac{1}{2}}$ dependence for the same reason.

For t=0.2 r.l. at 1 GeV, the path length simulation gives an energy resolution $\sigma_E/E=0.114$. Subtracting in quadrature the contribution from track counting (0.05) leaves a contribution $\sigma_E/E \approx 0.10$ from track obliquity alone.

3. Landau Fluctuations

At each electron energy the distribution of energy lost in the gaps is very asymmetric because of individual fluctuations bounded by the maximum delta ray energy lost in a gap. The estimated mean energy, therefore, shifts from the most probable toward the true mean and the resolution worsens as the number of samples increases. This introduces an additional nonlinearity with energy in the total simulated mean energy loss (Figure 8), and explains the departure of the energy resolution shown in Figure 9 from the $E^{-\frac{1}{2}}$ law for both Monte Carlo and measured data.

4. Comparison of Proportional Mode Simulations with Measurements

Figures 8 and 9 show that the Monte Carlo simulation of energy loss agrees well with the proportional mode measurements. The energy

dependence of the measured signal (Figure 8) does not, however, appear to show the small nonlinearity found in the simulation.

The agreement of the simulated and measured energy resolutions (Figure 9) is excellent. The increase of α at high energies is related primarily to the finite depth of the calorimeter. Other systematic effects may include also the nonlinearities in the evaluation of the Landau fluctuations. At low energies the measurements could not be carried far enough to check the simulation in the range most sensitive to the low electron energy cut-off.

C. Geiger Mode

1. Shower Characteristics and Energy Dependence

The Geiger mode calorimeter is not sensitive to local fluctuations in deposited energy (Landau effect), but it is sensitive to fluctuations from multicell response to oblique tracks and from saturation characterized by more than one track in a cell. The last effect can be studied in simulation in the zero gap width limit, which eliminates the path length fluctuations.

Because of saturation there are significant macroscopic differences in the structures of showers as seen by proportional and Geiger mode calorimeters. It is helpful to visualize the shower as made up of two components, an intense core with significant correlation among tracks and a soft halo with relatively little track correlation. At

1 GeV the Geiger mode shower is wider (by approximately twenty percent) and longer than for the proportional mode, and the response is more sensitive to what happens at the sides and end. Figure 10 shows the relevant longitudinal distribution. The Geiger mode calorimeter suffers more from marginal calorimeter depth; but it is less sensitive to losses in absorbing material ahead of the sensitive volume.

The effectiveness of the Monte Carlo program is verified by the good agreement shown in Figure 11 between simulated and measured depth-development of showers at 4 and 16 GeV. Figure 12 shows the energy dependence of the signals obtained from the Monte Carlo simulation and from the measurements. The only input to the Monte Carlo program for purposes of normalization was the measured cell efficiency. The agreement is very good below 2 GeV. At higher energies the simulation shows more nonlinearity than do the measurements. It is our belief that this difference is a consequence of the elimination in the EGS program of the low energy electrons, which are more diffuse and, therefore, contribute relatively less to the saturation.

Figure 13 shows the simulated and measured energy resolution constant α. At 1 GeV the agreement is satisfactory. At higher energies the simulation predicts poorer resolution than is measured. As verified by an additional simulation at 1 GeV this is a consequence of the severe cut on low energy electrons. When the total pulse heights and nonlinearity factors are corrected to the measured values, the energy resolutions are also brought into agreement. At very low energies the disagreement between measured and simulated resolutions probably comes

from experimental errors, such as calibration fluctuations and pedestal instabilities, which were not included in the simulation.

The most troublesome effect of saturation is nonlinearity in the energy dependence of the signal, because calibration at several energies is needed to establish this dependence. One consequence of nonlinearity is that partially overlapping showers from, say, two 4 GeV γ's do not give the same total signal as an 8 GeV γ. Also, because the showers appear to be broader, the ability of a given segmented calorimeter to identify individual showers is reduced.

2. Choice of Geiger Cell Size

An important reason for the Monte Carlo study was optimization of the cell size. Simulations were made for (wire, fiber) separations in millimeters of (5, 10), (5, 5), (5, 20) and (2, 10). The efficiencies, estimated from the standard functional shape given in Section IV.A above, were 0.72, 0.64, 0.76 and 0.72, respectively. The pulse heights and resolutions for various cell dimensions are compared in Figure 14 to those for the (5,10) case. At 16 GeV, where the non-linearity factors are largest, the ratios of non-linearities are 0.95, 1.04 and 0.94 for the (5,5), (5,20) and (2,10) cases, respectively. We notice that, as expected, the larger the cell area, the smaller the number of discharged cells and the larger the non-linearity factor. A cell with one dimension smaller than the gap size is subject to larger track obliquity fluctuations. Except at high energies the 5 x 10 mm^2 cell is a good choice. In general the best three dimensional cell shape is prob-

ably cubic.

3. Dependence on Angle of Incidence

Figure 15 shows the simulated calorimeter response to 1 GeV electrons incident at angles from 0 (normal incidence) to $\pi/3$. Results for different Geiger cell sizes and for operation in the proportional mode are shown. Only for the 2x10 mm^2 cell does the response depend strongly on shower obliquity. For the 5x10 mm^2 cell the number of discharged cells is essentially independent of angle. Hence the nonlinearity factor is independent of angle. When the angle increases from 0 to $\pi/4$, the energy resolution deteriorates by approximately 10 percent independent of energy and has the same pattern for all cell sizes and for the proportional mode.

V. TEST RESULTS

A. Method of Analysis

1. Electronic and Intrinsic Calibration

Each measurement of sense wire charge depended on electrical component values, sampling gate width and ADC sensitivity. The electronic calibration for each wire and strip channel was carried out as described in Section III. B above. Eighteen input (DAC) voltages were used to parameterize the response of each channel.

For the Geiger mode calorimeter, the energy determination is made by counting the total number of discharged cells (intrinsic calibration). Because of the excellent pulse height uniformity of the Geiger cells, the distribution of charge for each wire channel, summed over many events, shows a multipeak structure. For a typical wire channel distribution Figure 16 shows the Fourier transform, which gives the ratio S of corrected ADC counts to the number of discharged cells. Figure 17 shows the distribution of S for 28 wire channels for which S could easily be measured. The rms width $\sigma_S \approx 0.03$ S comes at least partly from channel to channel variations in the values of the calibration capacitors and the correction factors for the high voltage coupling capacitors. For the strip channels, for which the cell periodicity is washed out by geometry, we rely on the electronic calibration.

2. Energy Sums and Fits

The energy scale for the calorimeter is established by relating electron beam energy to the total number of discharged cells per event. The latter is obtained for each event by summing the corrected ADC counts over all wire (or strip) channels and then dividing by the value of S measured for the run. With this procedure the effects of small run to run fluctuations in voltage, pressure, temperature and gas mixture are negligible. Because all measurements were made with constant beam alignment, the event topologies were similar, so that the effects of the small channel to channel variations in sensitivity were also negligible. Figure 18 shows the distribution of measured total charge for electrons at each of four energies. These events have survived

criteria which eliminated most false triggers, pion contaminaton in the beam, multi electron triggers and events where the beam particle was not centered in the calorimeter.

For each such sample a Gaussian fit has been made to the binned histogram of charge Q, using a chi-squared minimization between two cut-off points chosen iteratively by the program. First the mean Q and rms width σ_Q of the included sample are calculated. Then events more than three standard deviations from the mean are eliminated. The process stops when the number of events eliminated in a step is $\leq 10^{-3}$ times the number in the remaining sample. The errors assigned to Q and σ_Q/Q are then $(N)^{-\frac{1}{2}}$ and $(2N)^{-\frac{1}{2}}$ respectively. No background subtraction was made. This gives a slightly conservative estimate of the resolution. The Gaussian fits are good except in the tails, which have the appearance of a smooth constant background.

3. Systematic Errors

Because the electronic hardware was not adequately cooled, some temperature dependent variations (mostly diurnal) occurred. We have made corrections for these where possible. A systematic error of 2 percent to account for gate-width variations, pedestal shifts, unmeasured channel to channel gain variations and other electronic instabilities was added in quadrature with statistical errors in obtaining all final errors.

B. Performance as a Function of Sense Wire Voltage and Gas Composition

For a range of beam energy E and sense wire voltage V and for gas mixtures with three and four percent (molar) ethyl bromide concentrations, the charge (ADC counts) Q, charge per cell S and number of cells N were measured and analyzed using the procedures outlined in Section V.A above. The results are presented in Tables I-III and Figure 19.

1. Voltage Dependence

Table I gives the voltage dependences for 4 GeV beam pions which did not interact in the first (18 layer) submodule. Selection criteria for individual pions required that each trajectory was nearly centered in the calorimeter. The pulse height distribution was fitted with a Gaussian superimposed on a smooth background. With the assumption that the peak Q corresponds to noninteracting particles at normal incidence crossing one cell per layer, the cell efficiency is given by $\varepsilon = Q/18\ S$. In the voltage range 1050-1112 volts Table I shows a constant value, $\varepsilon \approx 0.73$.

Table II shows the voltage dependence of measurements for 1 GeV electrons and 3 percent ethyl bromide. These data and those of Table I are plotted in Figure 19a. It shows that the voltage dependences of S at 3 and 4 percent ethyl bromide are identical, provided that the voltage scales are shifted relatively by 89.9 volts. This value was obtained from a fit to the measurements shown as a dashed curve in the

figure. The other parameters are given in the figure caption.

Figures 19b and 19c show that for constant electron energy and gas concentration the average number of cells increases and the pulse height resolution improves with increasing voltage. If this effect were associated entirely with a cell efficiency ϵ increasing with voltage, in contradiction with the results given in Table I, we would expect the energy resolution, which is the product of the pulse height resolution and the nonlinearity factor NLF $\equiv (dE/E)/(dQ/Q)$, to improve with increasing voltage as $\epsilon^{-\frac{1}{2}}$. If, on the other hand, higher voltage simply increases the probability of parasitic discharges of neighboring cells, the effective cell area increases with voltage, implying more saturation and a greater nonlinearity factor. In this case the energy resolution worsens with increasing voltage. Our limited measurements do not resolve this uncertainty.

2. Dependence on Gas Composition

At constant electron energy and corresponding voltages (i.e. those giving equal values for S) the number of cells N is inversely correlated with ethyl bromide concentration. Figure 19b shows that for 1 GeV electrons the number of cells is significantly ($\sim$15 percent) lower for the 4 percent ethyl bromide concentration. Whether this implies lower efficiency or reduced parasitic effects is not determined directly. The pulse height resolution is somewhat better for the 4 percent concentration. In addition the analysis of the data from Tables II and III shows that for the 4 percent measurements the

nonlinearity factor at 1 GeV is smaller in the ratio 1.05/1.08. This could indicate that parasitic effects are smaller at 4 percent.

We conclude that the energy resolution is not very sensitive to the ethyl bromide concentration in the 3-4 percent range, but 4 percent seems to exhibit reduced parasitic effects and improved linearity. The same effects are achieved by keeping the voltage very low.

C. Performance as a Function of Electron Energy

Table III summarizes calorimeter measurements for electron energies in the range 0.125-16 GeV. The operating voltages differed slightly from run to run; hence all data were corrected, using the S and Q dependences shown in Figure 19 and in Tables I and II, to values appropriate to a constant voltage, V=1094.4 volts. In the energy range 0.125-4 GeV the measured value of S is seen to be very constant as expected. For the narrow gate the small values of the cell periodicities were not accurately measurable. For these (higher energy) measurements, therefore, the average value of S measured with the wide gate [brackets in Table III] was used to calculate N. Table III shows also that measurements made with both gates at one energy (2 GeV) are consistent.

1. Nonlinearity with energy

Figure 20 shows that the number of cells discharged is not linear with electron energy. Above 4 GeV some nonlinearity is expected

because of the limited thickness (15.2 radiation lengths) of the calorimeter. The deviation at somewhat lower energies comes primarily from saturation associated with non-zero cell dimensions. The nonlinearity factor defined in Section V.B above and presented in Table III is calculated from the slope of a polynomial fit to the E vs Q data of Figure 12. Typically the deviation from linearity is 11 percent at 4 GeV.

2. Energy resolution

The fractional energy resolution shown in Table III and Figure 20b is the product of the pulse height resolution and the nonlinearity factor. Below 4 GeV it is empirically represented by $\sigma_E/E \approx 0.011 + 0.112\,[E(\text{GeV})]^{-\frac{1}{2}}$ Above 4 GeV the measured resolution is poorer than that given by this formula, at least partly because of shower leakage from the back of the calorimeter.

For reasons not entirely understood the electronics instabilities discussed in Section III above were found to be worse for the wire channels than for the strip channels. Hence the energy resolutions presented in Table IV are for strip channel measurements. The corresponding wire channel resolutions are systematically larger by as much as twenty percent. (See Table III.)

D. Shower Development in Depth

Table IV shows the summed pulse heights and resolutions measured

for one, two, three and four submodules (3.8, 7.6, 11.4 and 15.2 radiation lengths, respectively). The spectra and fits to the 12 GeV measurements are shown in Figure 21. Figure 22 shows that the nonlinearity factor is a strong function of both energy and calorimeter thickness. Figure 23 shows the development of the shower in depth indicating that at the highest energies the shower is not completely contained. Our Monte Carlo studies have shown that the energy missing is approximately half the energy seen in the last submodule. Figure 24 shows the energy resolution as a function of calorimeter thickness for five energies. For $E \leq 1$ GeV, i.e. for a very large majority of the electrons and photons from PEP and PETRA, the fourth submodule would contribute little to the energy resolution.

E. Correlation of Strip and Wire Channel Signals

Multiple stereo projections using the same set of gaps provide a powerful constraint to help isolate individual showers in a multiple shower event. This is a direct consequence of local charge conservation, i.e. in each gap the induced charge on the cathode strips is (nearly) equal to the electronic charge collected on the sense wires.

Figure 25 shows for 1 and 4 GeV electrons the distributions of the ratios of signals induced on the upstream A and downstream B cathode strips in the first submodule. The rms widths are only 1-2 percent. Each ratio is approximately unity, as expected. The 4 percent average deviation of the ratio from unity (Table V) may be caused by an

asymmetry in the average sense wire position in the gap and/or component differences in the calibration circuits.

For each event we have calculated also the ratio of strip channel to wire channel signals, both for the first submodule and for the full calorimeter (Figure 26 and Table V). The corresponding distribution widths (~3 percent) are significantly greater than for the strip (A/B) ratios. Also the distributions are asymmetric, a consequence of the greater instabilities observed for the wire channel electronics. The average ratio of strip to wire signals is less than unity by ~10 percent.

For all the measured signal ratios the widths are far less than the corresponding energy resolutions given in Table IV (80-90 percent for the first submodule and 6-12 percent for the full calorimeter). We infer, therefore, that a stereo system with multiple views from the same set of gaps provides far more information to eliminate multiple shower ambiguities than one based on the use of alternate gaps for different views.

F. Operation in the Proportional Mode

Measurements were made for proportional mode operation at one atmosphere with incident electrons at five different energies and with 1 GeV electrons at five different gas pressures. Figure 27 shows the pulse height spectra for electrons with 0.25 and 4 GeV, respectively. The background from false triggers, track pileup and noise has been

subtracted to obtain the signal levels and resolutions given in Table VI. Figure 28a shows that for the full calorimeter the signal is linear with energy up to 8 GeV, even though some leakage from the back of the calorimeter is expected at the highest energies. The slight deviation from linearity at 0.25 GeV may result from the 5 percent uncertainty in the beam energy in this region.

The energy resolution shown in Figure 28b may be parameterized for the 15.2 radiation length calorimeter as $\sigma_E/E = 0.023 + 0.105\,[E(\text{GeV})]^{-\frac{1}{2}}$ where the energy independent term comes from systematic errors (electronic calibration instabilities, etc) and, as discussed above, from the Landau fluctuations. (See Section IV.B.3.)

Omitting signals from the fourth submodule gives the performance of an 11.4 r.l. calorimeter. Below 1 GeV this is the same as for the full (15.2 r.l.) calorimeter. At the higher energies, as shown in Table VI, the pulse height resolution for the shorter calorimeter deteriorates significantly.

Figure 28b shows also the resolution measurements made with one radiation length of aluminum ahead of the calorimeter. At 0.25 GeV the signal is small and the background subtraction is very difficult.

Also for the proportional mode the ratios of signals on the electrodes of the first submodule were measured. (Figure 29). The rms widths of the distributions for both strip to strip and strip to wire ratios were 8 percent, compared with 2 and 3 percent, respectively,

for the Geiger mode. The considerably poorer correlation of the proportional mode signals is attributed to noise.

For 1 GeV electrons the pressure dependence of the energy resolution was measured (Figure 30). The sense wire voltage was varied as necessary to keep the ADC's in range. The improvement of energy resolution with increasing pressure comes from a larger signal to noise ratio, reduced Landau fluctuations and increased gas scattering, which minimizes the effect of oblique tracks.

A transverse position scan verified that the calorimeter response was insensitive to displacement of the beam. For several displacements up to one channel width, the total signal was found to be constant within the rms error of less than one percent. The energy resolution was constant within the rms error of approximately three percent.

These results are generally consistent with those of an extended series of proportional mode calorimeter tests by the UCLA group.[8]

VI. CONCLUSIONS

In gas sampling calorimeters for electrons below a few GeV, Geiger mode operation has important advantages over proportional mode operation. It gives a better signal to noise ratio and the required analogue electronics is simpler. The cell structure provides a convenient method for intrinsic calibration. In addition, the strong correlation between anode wire and induced cathode signals can be used

to provide valuable constraints for the reconstruction of complex event topologies.

At 1 GeV the Geiger mode gives slightly (~10 percent) better energy resolution than the atmospheric proportional mode. At energies well above 1 GeV the Geiger mode suffers from saturation, leading to both loss of energy resolution and nonadditivity of shower energies. For the gap width of 5 mm with comparable cell dimensions, which has been shown by Monte Carlo to be the optimum shape, this deterioration is acceptable for electron energies up to at least 16 GeV.

We have shown that for gas calorimeters the fluctuations in track obliquity and the Landau effect contribute to the energy resolution more than do fluctuations in the number of tracks. Although Geiger mode discharges are not sensitive to Landau fluctuations, a nearly equivalent contribution to the resolution comes from cell inefficiency and saturation. Our results provide evidence for and explanation of the fact that the energy resolutions of typical gas sampling calorimeters are approximately twice the values predicted by simple track counting.

Acknowledgments

The availability of the SLAC C-Beam and the help of Roger Gearhart were essential to the tests undertaken here. We thank the UCLA group for loan of the computer and much of the electronics. R. Koda gave assistance during the set-up, and J. Kubic deserves special thanks for

the software and operating instructions. Finally, the entire program could scarcely have been undertaken without the help of Fred Goozen, who made the laminates, constructed the calorimeter and participated in almost all phases of the test operations.

References

1. L. Federici, M. Nardi, F. Ceradini and M. Conversi. Nucl. Instr. and Meth 151 (1978) 103-105.

2. H.G. Stever, Phys. Rev. 61, 38 (1942).

3. G. Charpak and F. Sauli. Nucl. Instr. and Meth 96 (1971) 363.

4. Roger A. Gearhart. Test Beam Facility, March 27, 1978. Unpublished.

5. The EGS Code System: Computer Programs for the Monte Carlo Simulation of Electromagnetic Cascade Showers (Version 3) by Richard L. Ford and W.R. Nelson, SLAC Report No. 210 (June 1978).

6. K.A. Isperian, A.T. Mergerian and A.M. Zverev, Nucl. Instr. and Meth. 117 (1974) 125.

7. F. Harris, T. Katsura, S. Parker, V.Z. Peterson, R.W. Elsworth, G.B. Yodh, W. Allison, C.B. Brooks, J.H. Cobb, and J.H. Mulvey. Nucl. Instr. and Meth. 107 (1973) 413.

8. UCLA High Energy Experimental Group Notes. Unpublished. See, for example, J. Spahn and C. Buchanan, Comments on Model A Analysis Figures, HEE-103, Dec. 12, 1978. Also, J. Kubic, Model A Calorimeter Monte Carlo Program, HEE-158, Feb. 2, 1981. Also, J. Spahn, Model A and B Calorimeters, HEE-159, Feb. 11, 1981. Also W. Slater et al. Exposure of the South Poletip Calorimeter to a Test Beam, HEE 163, Oct. 15, 1981.

Table I - Measured response of first submodule (18 layers) to noninteracting 4 GeV pions at different voltages. The ethyl bromide concentration was four percent.

Voltage	Pulse Height, Q	Counts per Cell, S	Number of Cells, N	Cell Efficiency, ε
1001.8	14.0±3.6	--	--	--
1049.7	68.4±4.9	5.31±0.17	12.9±1.0	0.72±0.06
1094.2	134.3±5.4	10.2 ±0.23	13.1±0.6	0.73±0.03
1099.7	146.2±5.6	11.11±0.25	13.2±0.5	0.73±0.03
1111.7	164.9±5.8	12.47±0.27	13.2±0.5	0.73±0.03

Table II - Measured response of full calorimeter (72 layers) to electrons as function of voltage and energy. The ethyl bromide concentration was three percent.

Energy (GeV)	Voltage (Volts)	Pulse Height, Q	Resolution σ_Q/Q	Counts per cell S	Number of cells N
1	932.1	474±10	0.154±0.006	2.94±0.10	161.2±5.7
1	952.1	819±16	0.143±0.005	4.42±0.12	185.3±5.0
1	972.0	1264±25	0.134±0.005	6.56±0.14	192.7±4.2
1	992.1	1766±35	0.129±0.005	8.92±0.21	198.0±4.6
1	992.4	1765±35	0.128±0.006	8.75±0.21	201.7±4.8
1	1015.0	2428±50	0.127±0.005	11.39±0.28	213.2±5.4
1	1037.0	3215±64	0.118±0.005	14.58±0.32	220.5±4.9
0.5	992.2	871±17	0.160±0.008	8.50±0.19	102.5±2.2
4	992.2	5801±116	0.079±0.004	8.64±0.19	671.4±14.9

Table III - Measured response of full calorimeter (15.2 r.l.) to electrons. Q and S have been corrected for small differences in operating voltage. For the data taken with the narrow sampling gate, S (in brackets) was not measured. An average S from measurements at other energies has been used to calculate N. Values of σ_Q/Q, the nonlinearity factor, NLF and σ_E/E are for wire channel data. The ethyl bromide concentration was four percent. For the 2 GeV measurements W and N refer to the wide and narrow sampling gate, respectively.

Energy (GeV)	Pulse Height, Q (counts)	Pulse Height per cell, S (counts)	Number of cells N	Resolution σ_Q/Q (percent)	Nonlinearity Factor NLF	σ_E/E (percent)
0.125	264±9	9.97±0.24	26.5±1.0	34.4±1.3	1.008	34.7±1.4
0.25	476±13	9.97±0.24	47.7±1.5	23.2±0.8	1.013	23.5±0.8
0.5	900±21	9.99±0.22	90.1±2.2	17.4±0.6	1.024	17.8±0.6
1	1843±42	9.97±0.24	184.9±4.9	12.4±0.4	1.048	13.0±0.4
2 W	3418±77	10.01±0.23	341.6±8.6	9.7±0.3	1.082	10.5±0.3
2 N	3497±85	[10.00±0.23]	[349.7±11.6]	9.3±0.3	1.082	10.1±0.3
4	6575±145	10.18±0.25	645.8±21.3	6.6±0.3	1.137	7.5±0.3
8	12197±271	[10.00±0.24]	[1219.7±32.1]	5.5±0.2	1.199	6.6±0.2
12	16558±367	[10.00±0.24]	[1655.8±43.5]	5.2±0.2	1.211	6.3±0.2
16	21052±470	[10.00±0.25]	[2105.2±55.9]	5.0±0.3	1.250	6.3±0.2
	With one radiation length of aluminum ahead of calorimeter					
0.125	96.7±5.1	--	--	60.9±6.8	0.88	53.6±6.0
0.5	390±10	--	--	20.8±0.7	0.91	18.9±0.6
1	846±18	--	--	13.0±0.4	0.96	12.5±0.4

Table IV - Measured signal, pulse height and energy resolution versus depth. The ethyl bromide concentration was four percent. The symbols are the same as in Table III. The strip signals are used here.

E(GeV)	1 Submodule (3.8 r.l.) Q (counts)	σ_Q/Q (percent)	NLF	σ_E/E (percent)	2 Submodules (7.6 r.l.) Q (counts)	σ_Q/Q (percent)	NLF	σ_E/E (percent)
.125	166±7	44.6±2.1	1.52	67.8±3.2	220±11	36.4±1.9	1.055	38.4±2.0
.25	267±7	36.2±1.3	1.77	64.1±2.3	406±9	26.3±.9	1.093	28.8±1.0
.50	374±9	37.9±1.3	1.88	71.3±2.4	715±16	20.8±.7	1.145	23.8±.8
1.0	547±12	37.3±1.3	2.15	80.2±2.8	1342±28	18.7±.6	1.255	23.5±.8
2.0 W	696±16	38.6±1.2	2.21	85.3±2.7	2193±46	19.1±.6	1.340	25.6±.8
2.0 N	799±21	33.0±1.2	2.21	72.9±2.7	2332±48	17.9±.6	1.385	24.8±.8
4.0	958±27	36.4±1.7	2.46	89.5±4.2	3806±83	16.6±.7	1.512	25.1±1.1
8.0	1280±30	35.4±1.2	2.78	98.4±3.3	5913±120	19.0±.6	1.619	30.8±1.0
12.0	1477±35	34.8±1.3	2.83	98.5±3.7	7371±156	18.8±.7	1.641	30.9±1.2
12.0	1466±34	34.1±1.2	2.87	97.9±3.4	7385±151	19.4±.6	1.643	31.9±1.0
16.0	1617±37	36.4±1.3	2.89	105.2±3.8	8621±181	20.2±.7	1.657	33.5±1.2

E(GeV)	3 Submodules (11.4 r.l.) Q (counts)	σ_Q/Q (percent)	NLF	σ_E/E (percent)	4 Submodules (15.2 r.l.) Q (counts)	σ_Q/Q (percent)	NLF	σ_E/E (percent)
.125	232±14	34.4±2.1	1.012	34.8±2.1	226±15	34.1±2.4	1.005	34.4±2.4
.25	443±14	22.9±1.0	1.022	23.4±1.0	436±17	21.9±1.0	1.010	22.1±1.0
.5	793±17	17.3±.6	1.035	17.9±.6	789±17	16.4±.6	1.016	16.7±.6
1.0	1628±35	12.6±.4	1.074	13.5±.4	1649±36	11.4±.4	1.035	11.8±.4
2.0 W	2881±60	10.8±.3	1.115	12.0±.3	2986±63	9.1±.3	1.058	9.6±.3
2.0 N	3041±62	10.4±.3	1.128	11.7±.3	3162±67	8.6±.3	1.065	9.2±.3
4.0	5421±112	8.0±.4	1.204	9.6±.5	5778±118	5.7±.3	1.108	6.3±.3
8.0	9709±195	8.6±.3	1.327	11.4±.4	10995±221	5.1±.2	1.195	6.1±.2
12.0	12879±257	8.8±.3	1.384	12.2±.4	15211±306	4.5±.2	1.249	5.6±.2
12.0	12902±257	8.7±.3	1.385	12.1±.4	15118±298	4.6±.2	1.246	5.7±.2
16.0	15308±306	10.0±.4	1.407	14.1±.6	18530±371	4.6±.2	1.277	5.9±.3

Table V - Measured ratios of signals on upstream A and downstream B strip channels of first submodule. Also shown are the measured ratios of signals on all strip channels and wire channels in the first submodule and full calorimeter. Values in parentheses represent the rms widths (in percent) of Gaussians fitted to the distributions of Figures 25 and 26, with their statistical errors. The ethyl bromide concentration was four percent.

Ratio (rms error)	Submodule I (3.8 r.l.)		Full Calorimeter (15.2 r.l.)	
	1 GeV	4 GeV	1 GeV	4 GeV
STRIPS (A/B)	1.04 (1.8±0.1)	1.04 (1.4±0.1)	-- --	-- --
STRIPS/WIRES	0.91 (2.6±0.1)	0.91 (3.1±0.1)	0.90 (3.6±0.1)	0.90 (2.5±0.1)

Table VI. Measured response of proportional mode calorimeter. The gas is Argon (90%)-CH4 (10%) at one atmosphere. The tests are described in the text.

	15.2 r.l.			11.4 r.l.
Beam Energy (GeV)	Signal (Relative)	P.H. Res. (%) No absorber	P.H. Res. (%) 1 r.l. aluminum	P.H. Res. (%) No absorber
0.25	79.0±0.5	23.0±0.8	42.0±1.4	--
0.5	144.2±0.7	18.4±0.5	21.2±0.6	--
1	286±1	12.8±0.3	14.2±0.45	--
4	1159±3	7.35±0.2	--	9.75±0.35
8	2370±6	6.0±0.2	--	9.0±0.3

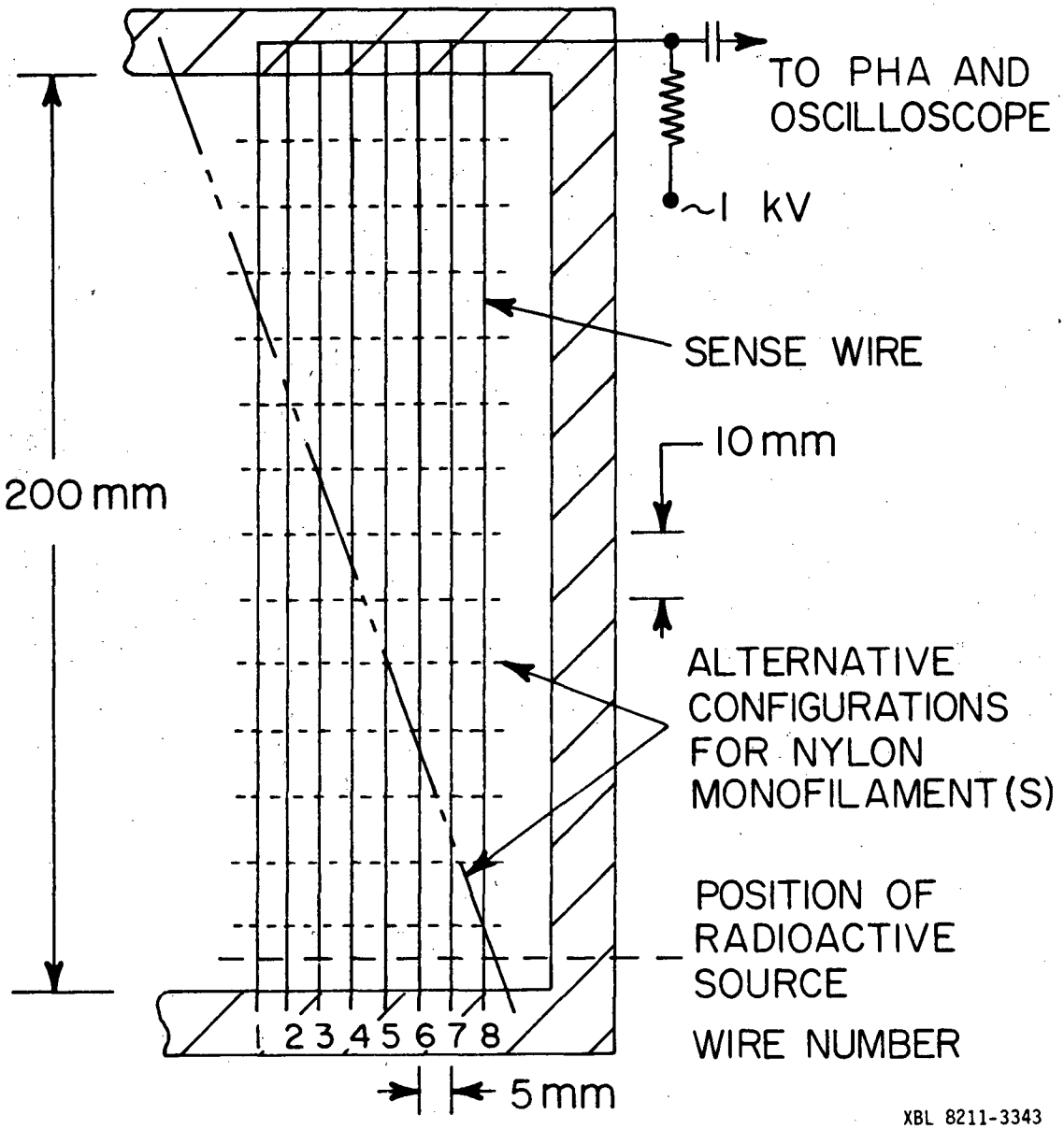

FIGURE 1. Composite plane for Geiger mode bench tests. The anode wires of 0.02 mm-diam. gold-plated tungsten are spaced 5 mm apart. The anode to cathode plane separation is 2.5 mm. Broken lines show two alternative positions of 0.05 mm diameter nylon monofilaments used to segment the chamber.

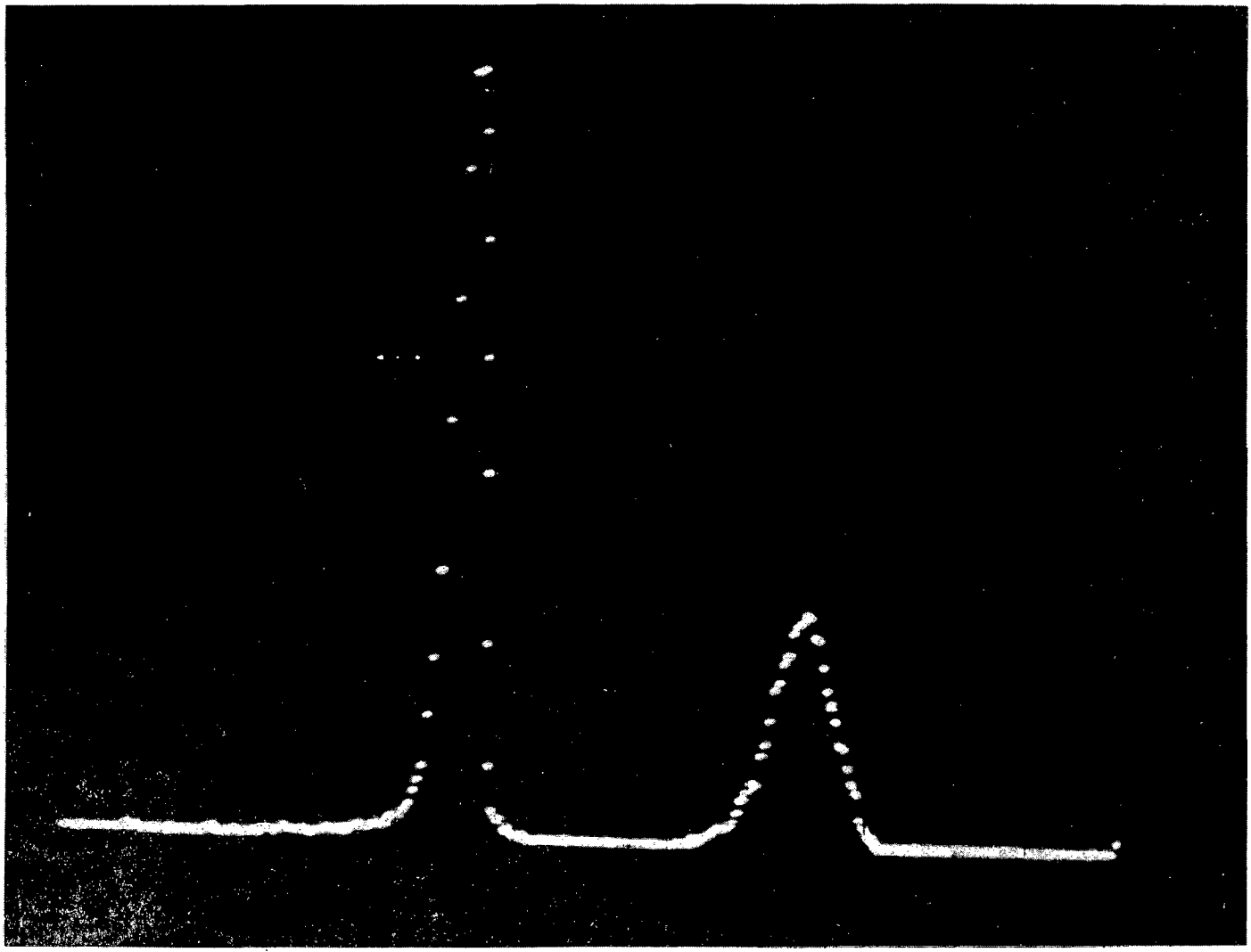

XBB 827-5867

FIGURE 2. Geiger pulse height spectrum for Fe^{55} source with 200 mm long (unsegmented) wire. Sometimes a neighboring wire is also dicharged giving twice the unit pulse height.

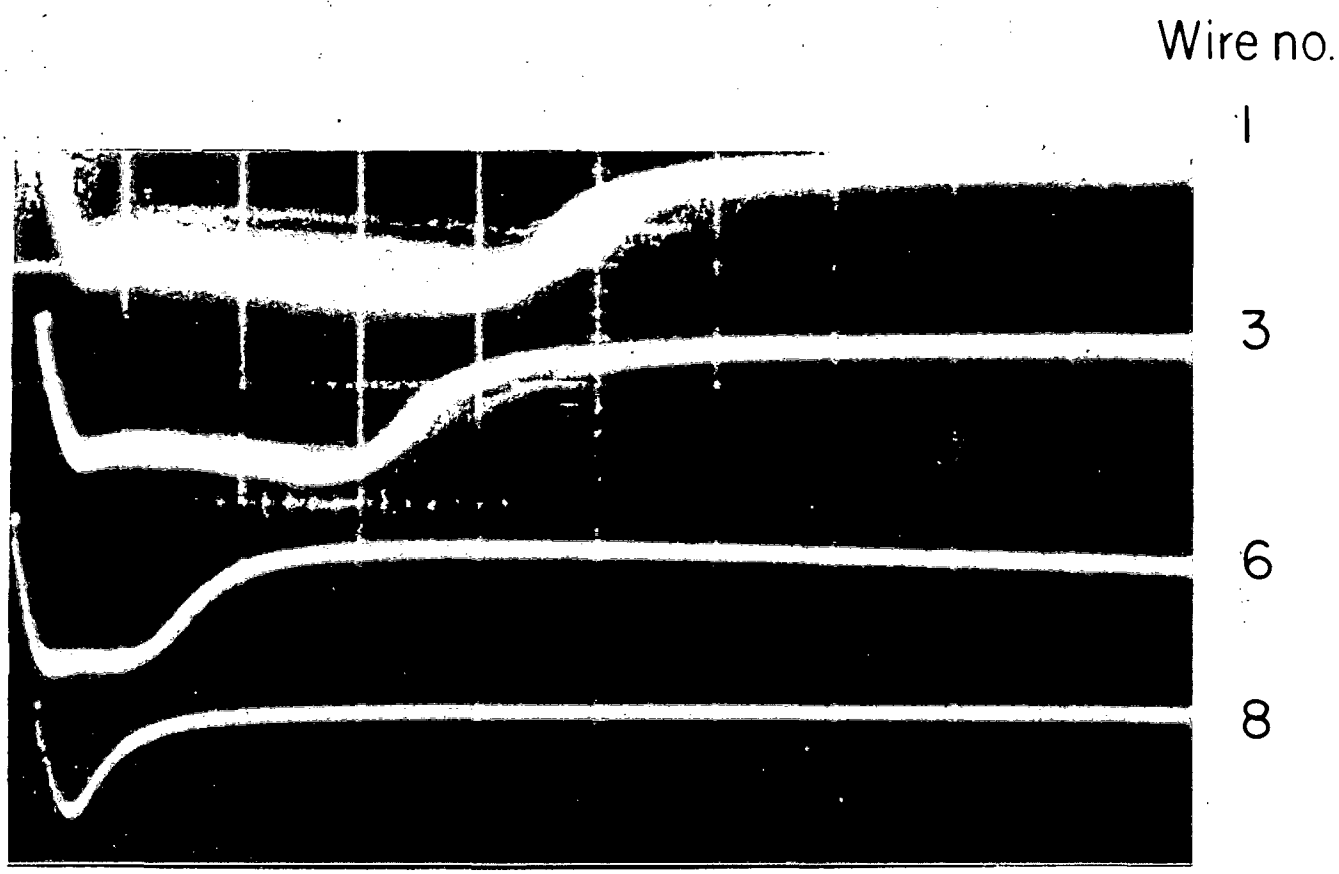

XBB 820-9784

FIGURE 3. Geiger pulse characteristic for wires terminated by a diagonal nylon monofilament as shown in Figure 1. The horizontal scale is 0.5 microseconds per large division. The vertical scale is 0.5 ma per large division.

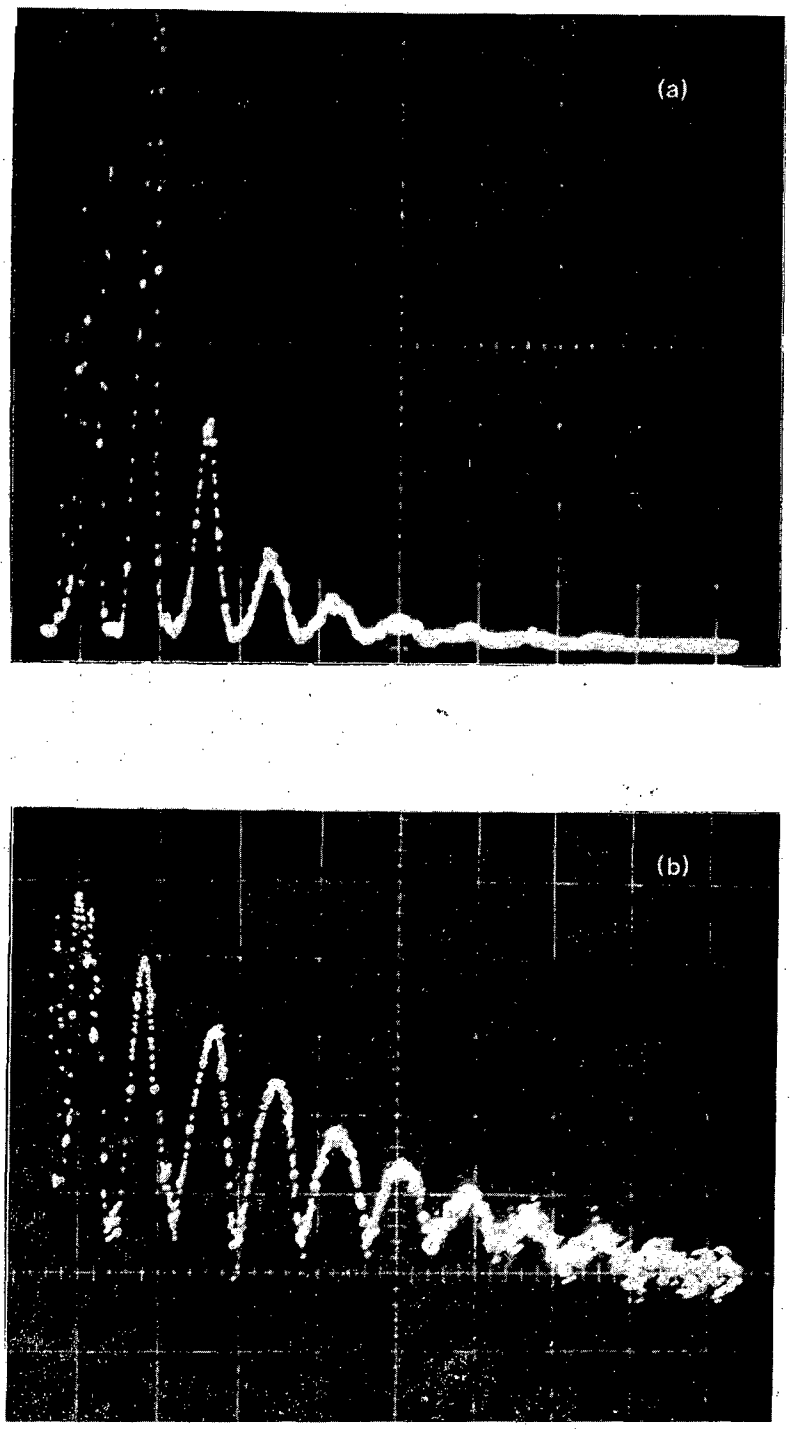

XBB 827-5869A

FIGURE 4. Pulse height spectrum using diffuse β-source for all wires of the chamber of Figure 1, segmented into 5 x 10 mm^2cells. a) The vertical scale is linear. b) The vertical scale is logarithmic.

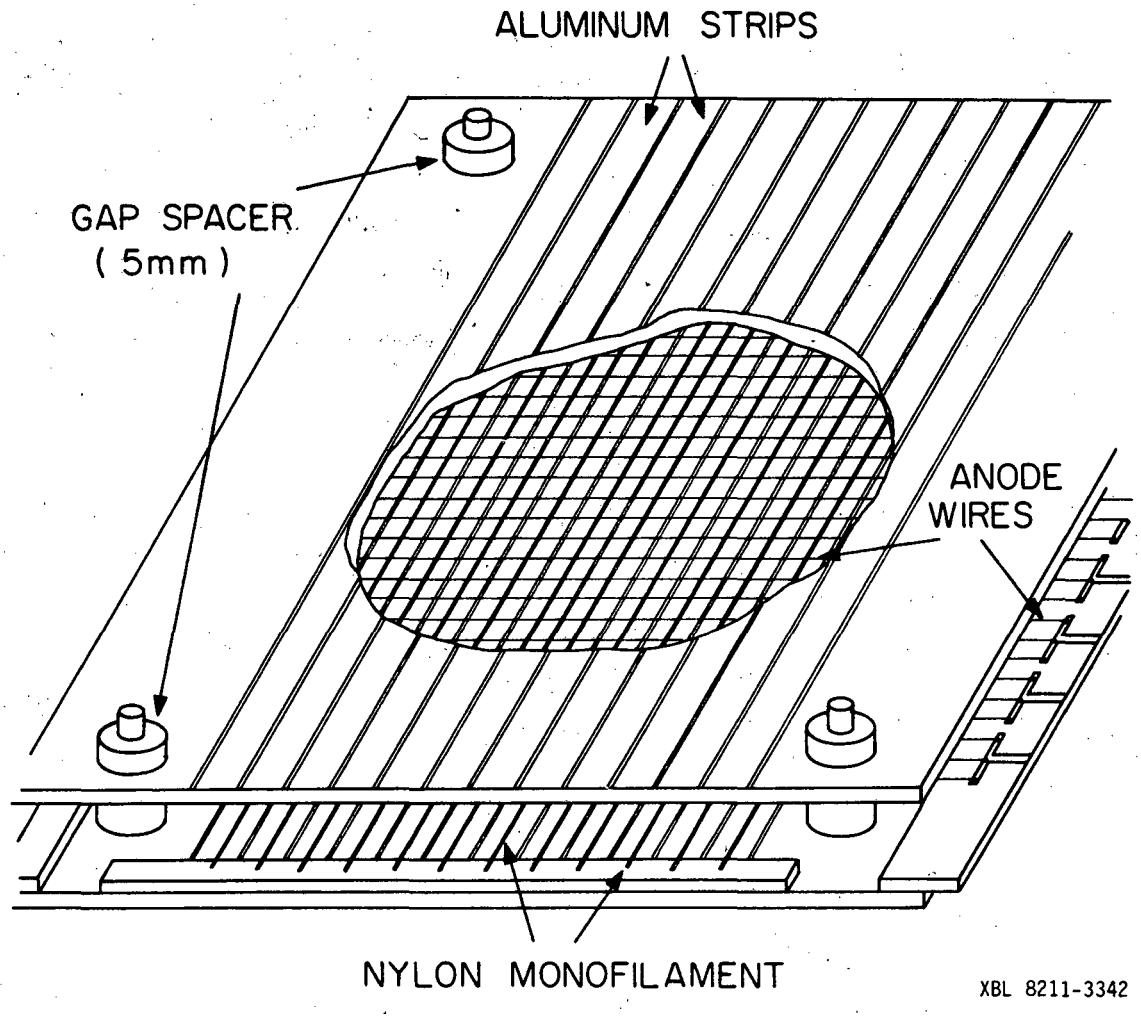

FIGURE 5. A section of a calorimeter layer showing the laminate and wire plane assembly. This configuration was also used in single plane tests.

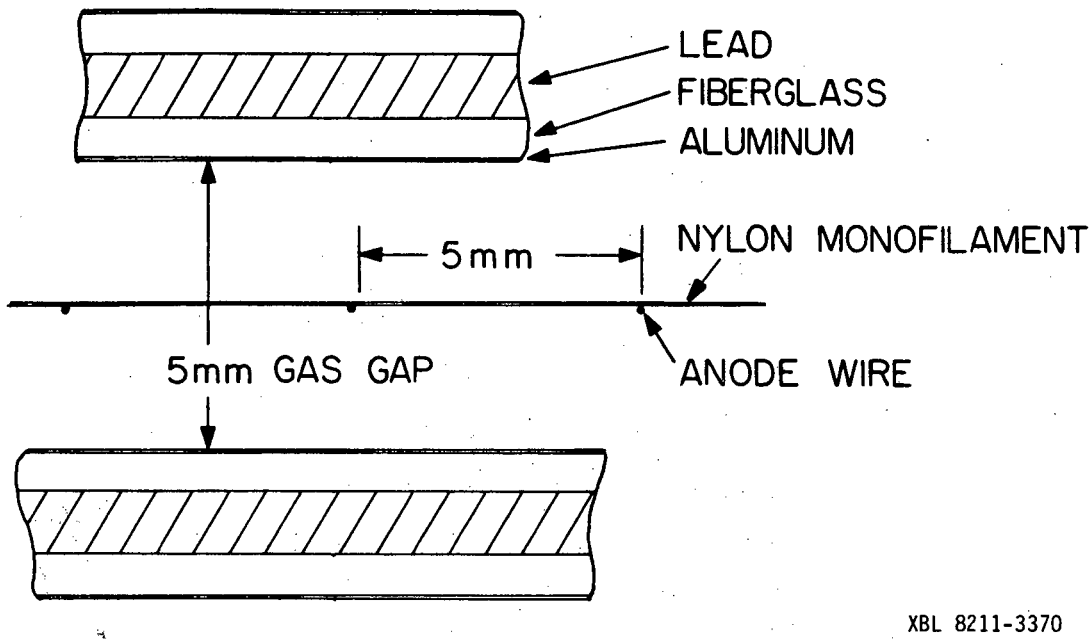

FIGURE 6. Details of laminate and gap. Thicknesses of aluminum, fiberglass and lead are 0.05 mm, 0.7 mm and 1.1 mm, respectively. Other parameters are given in the text.

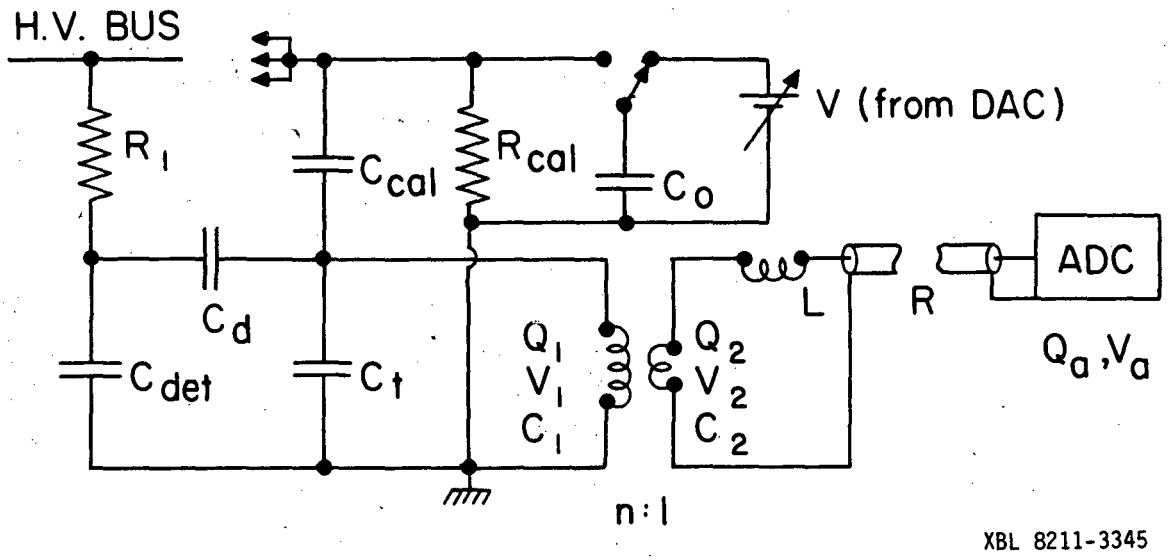

FIGURE 7. Sense wire calibration and peaking circuits for Geiger mode operation. Q, V and C subscripts 1, 2 and a refer to values at the input and output of the transformer and at the ADC, respectively. R=50 ohms, R_{cal}=3.3 ohms, L=47μHy, C_o=4μf, C_{cal}=470 pf and V=0.0125-10 volts (set by computer controlled DAC). For the wire channels R_1=2 x 10^7 ohms, C_d=5nf and n=6.3. C_t was chosen for each channel to make C_1=1.88 nf. For the strip channels R_1=C_d= ∞ , C_t=0, n=2.25, 3.2 or 4.5 as needed to match channel capacitances of 14.8, 7.4 and 3.7 nf, respectively.

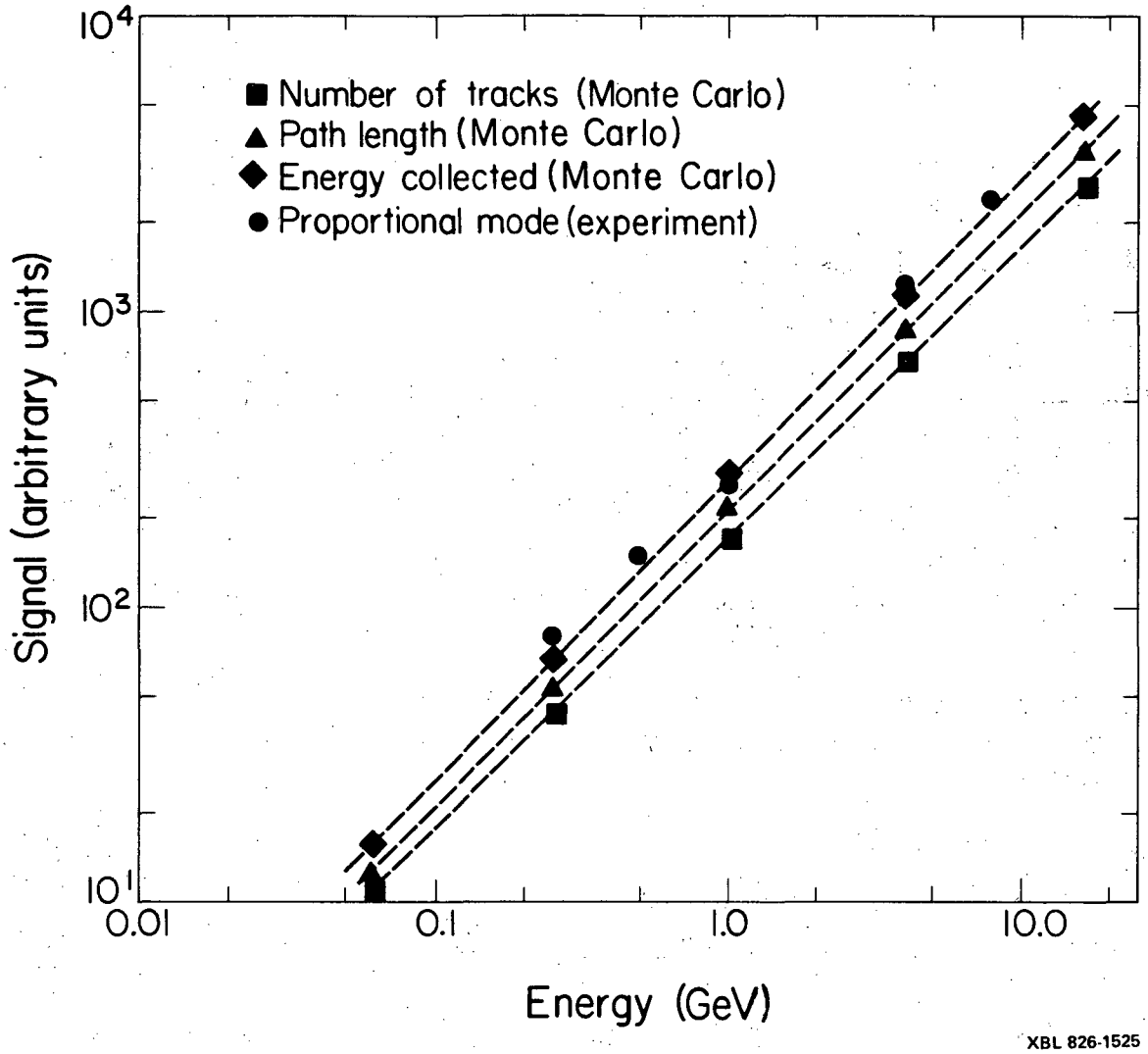

FIGURE 8. Monte Carlo simulation of the response of the 72-layer test calorimeter to electrons of various energies. Average number of tracks, path length and energy loss are shown. The straight lines are to guide the eye. Proportional mode measurements at one atmosphere are also included.

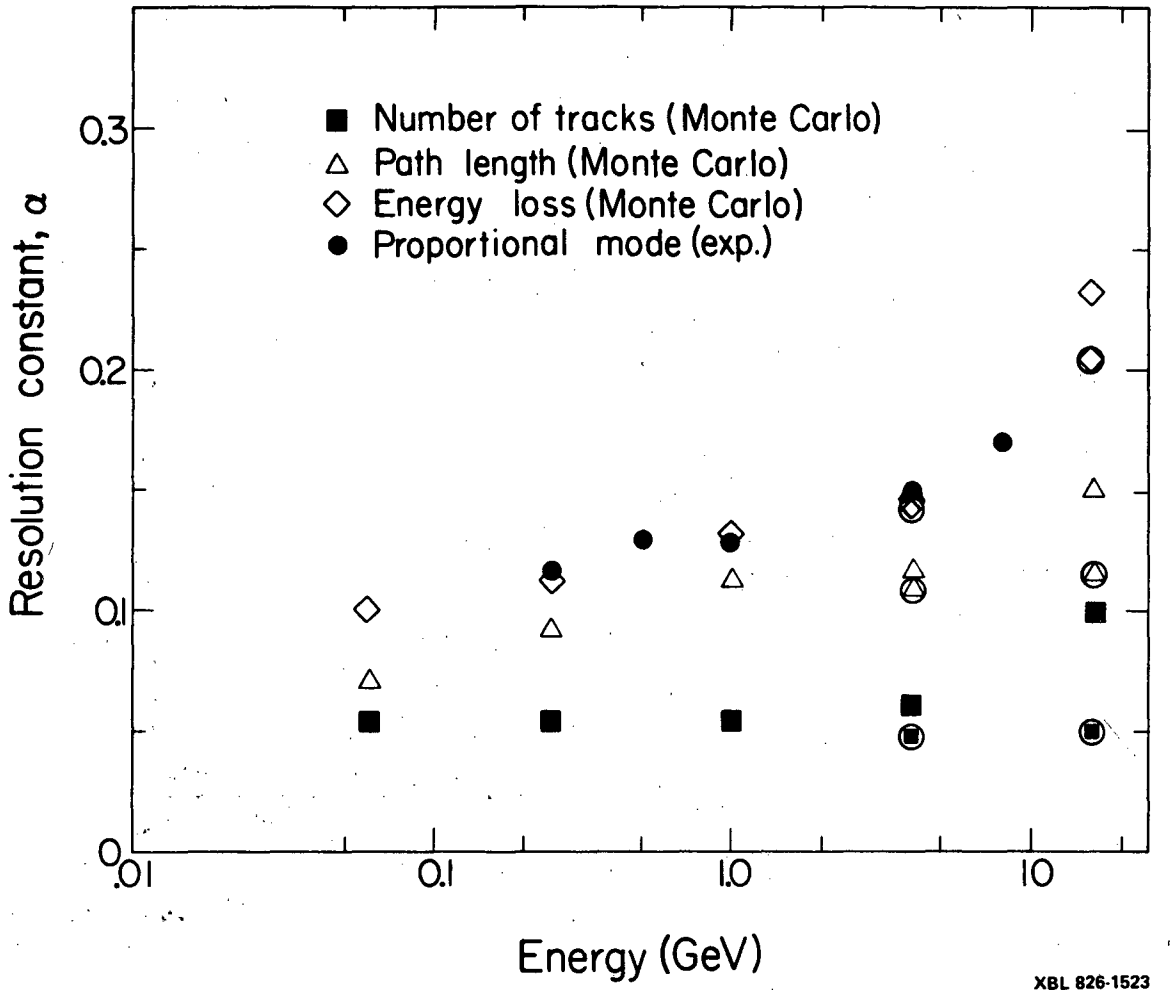

FIGURE 9. Monte Carlo simulation of energy resolution for 72-layer (15.2 r.l.) test calorimeter. The resolution constant α is defined in the text. Results for number of tracks, path length and energy loss are shown. Points surrounded by circles are simulations for a 21 r.l. (100 layer) calorimeter. The Monte Carlo points at 16 GeV have statistical errors of 5 percent. At lower energies the errors are smaller than the symbols. Proportional mode measurements at one atmosphere are also included.

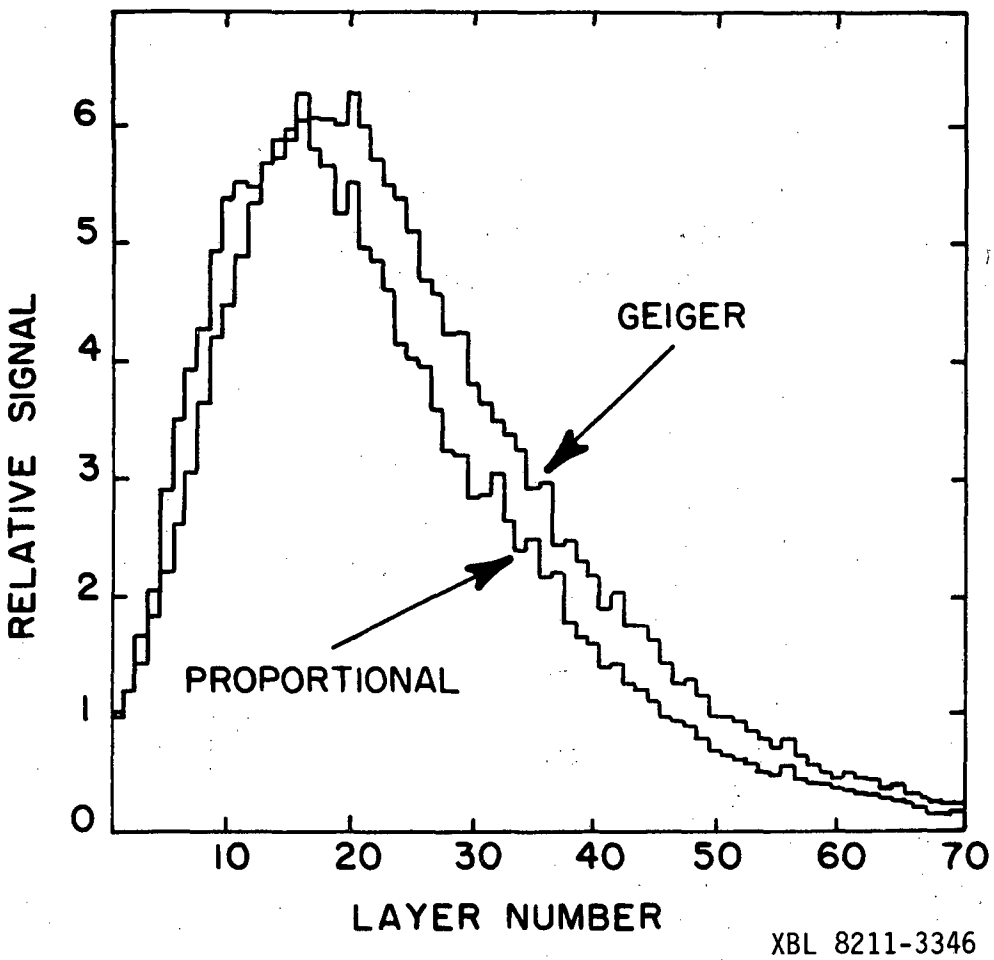

FIGURE 10. Simulated longitudinal shower distribution for 1 GeV electrons. For the porportional mode the energy loss distribution is shown. For the Geiger mode the distribution is of dischaged 5x10 mm^2cells.

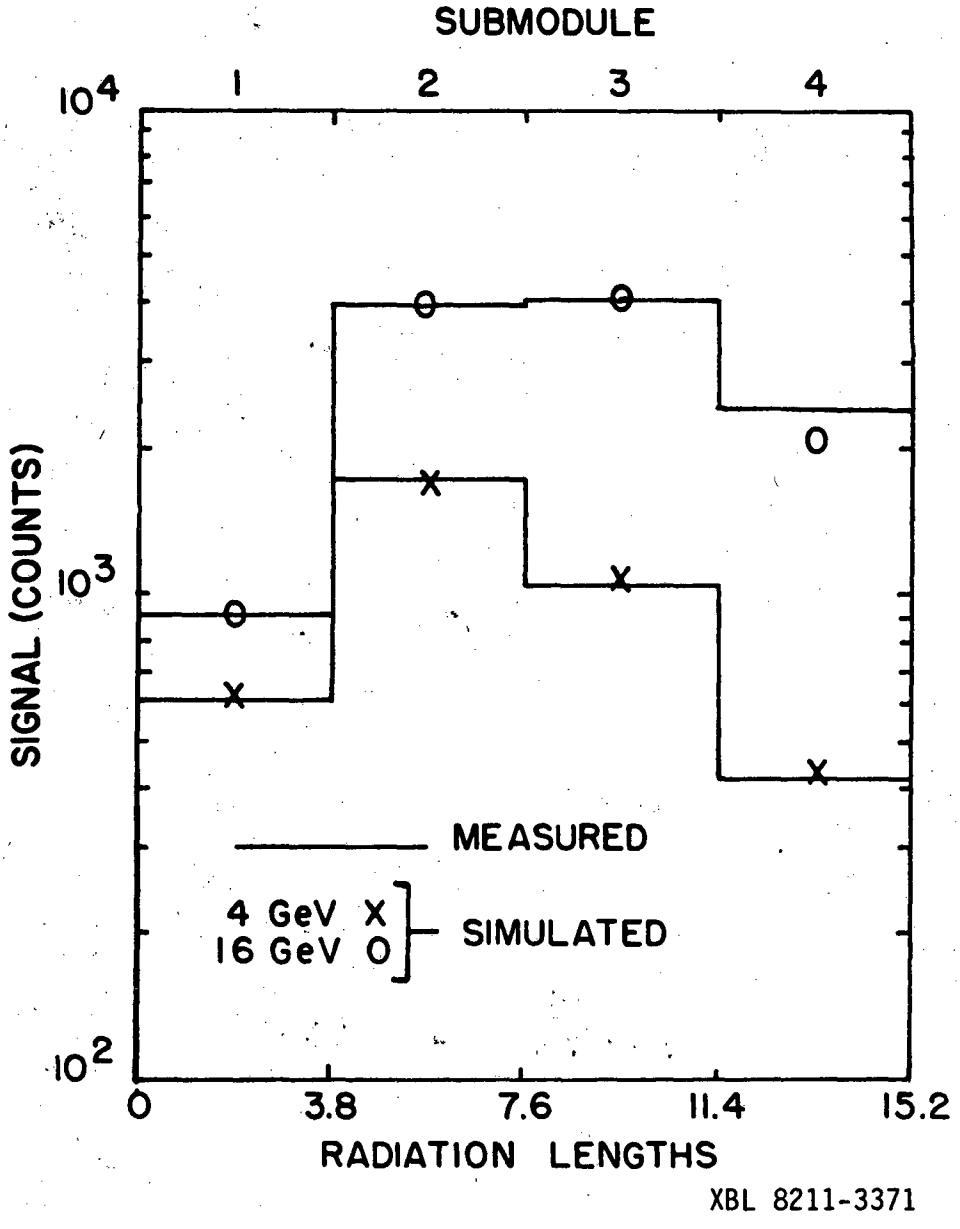

FIGURE 11. Simulated and measured Geiger mode shower development in depth for two values of the electron energy. Each level is the measured signal in a submodule. The points are simulated values.

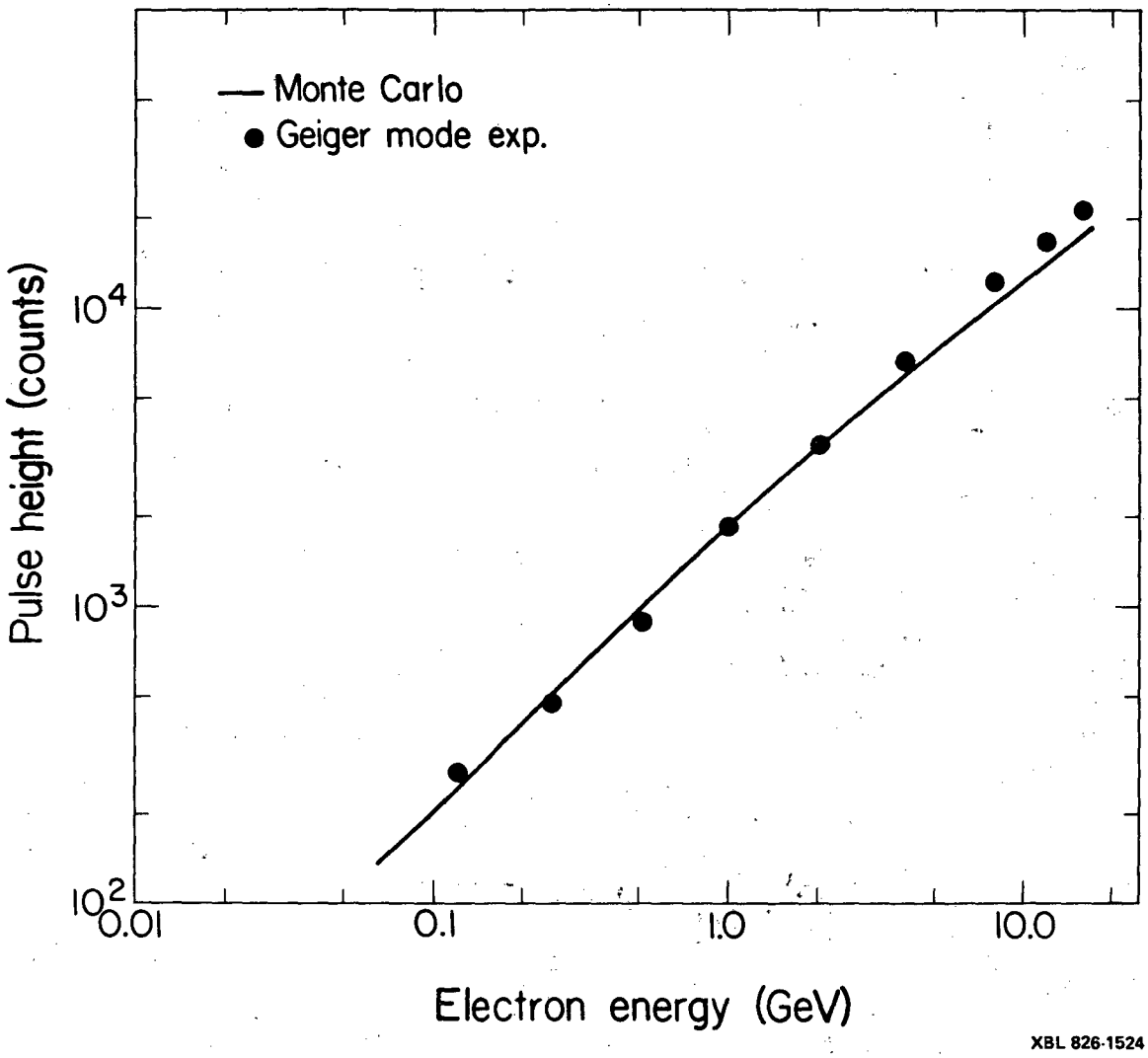

FIGURE 12. Average pulse height vs energy for 15.2 r.l. Geiger mode calorimeter. The measurements are points and the simulation is the solid line.

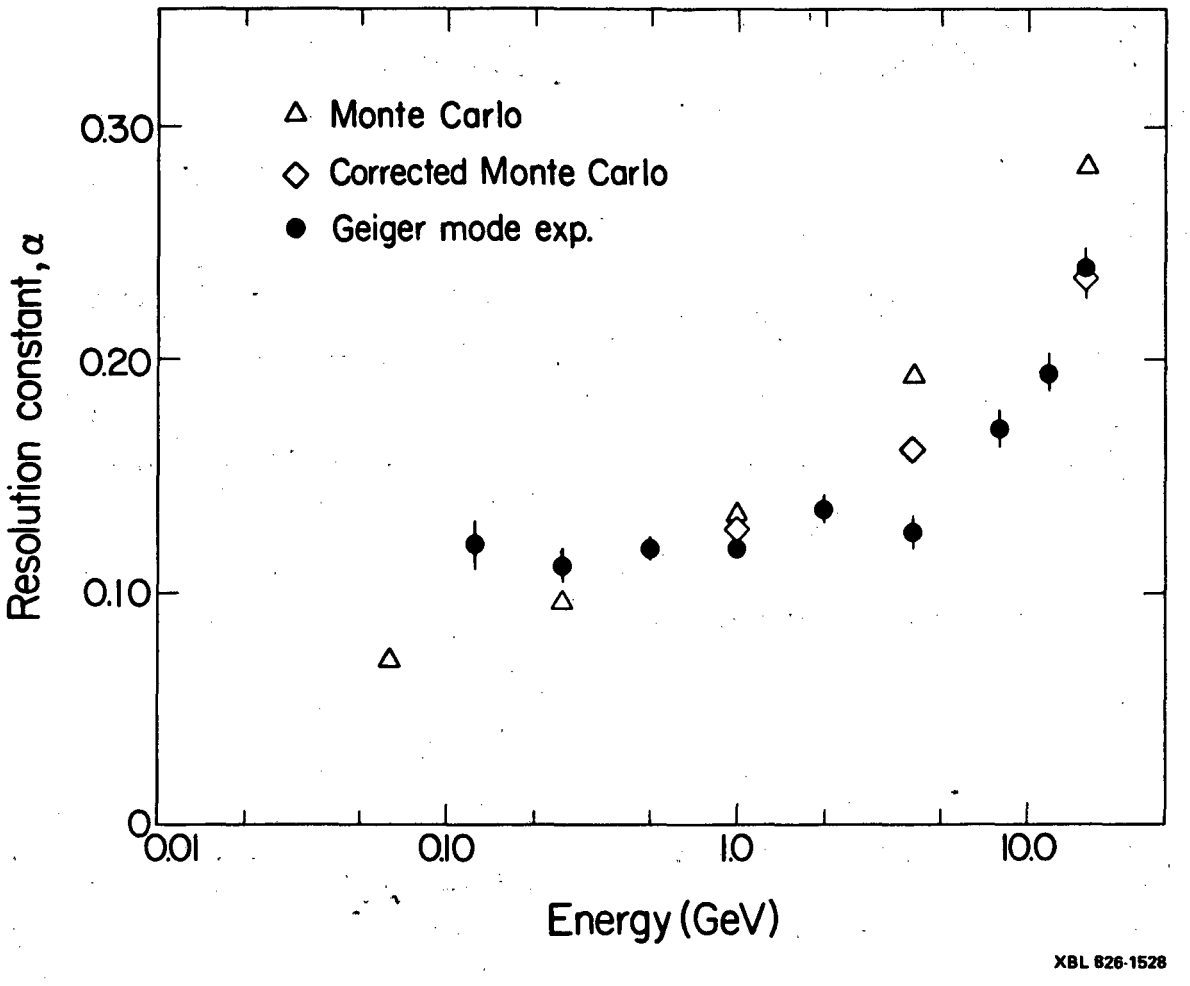

FIGURE 13. Energy resolution for Geiger mode operation. The different symbols refer to cathode strip measurements, uncorrected (raw) simulation and simulation corrected as described in text for loss of low energy electrons. See text for definition of α.

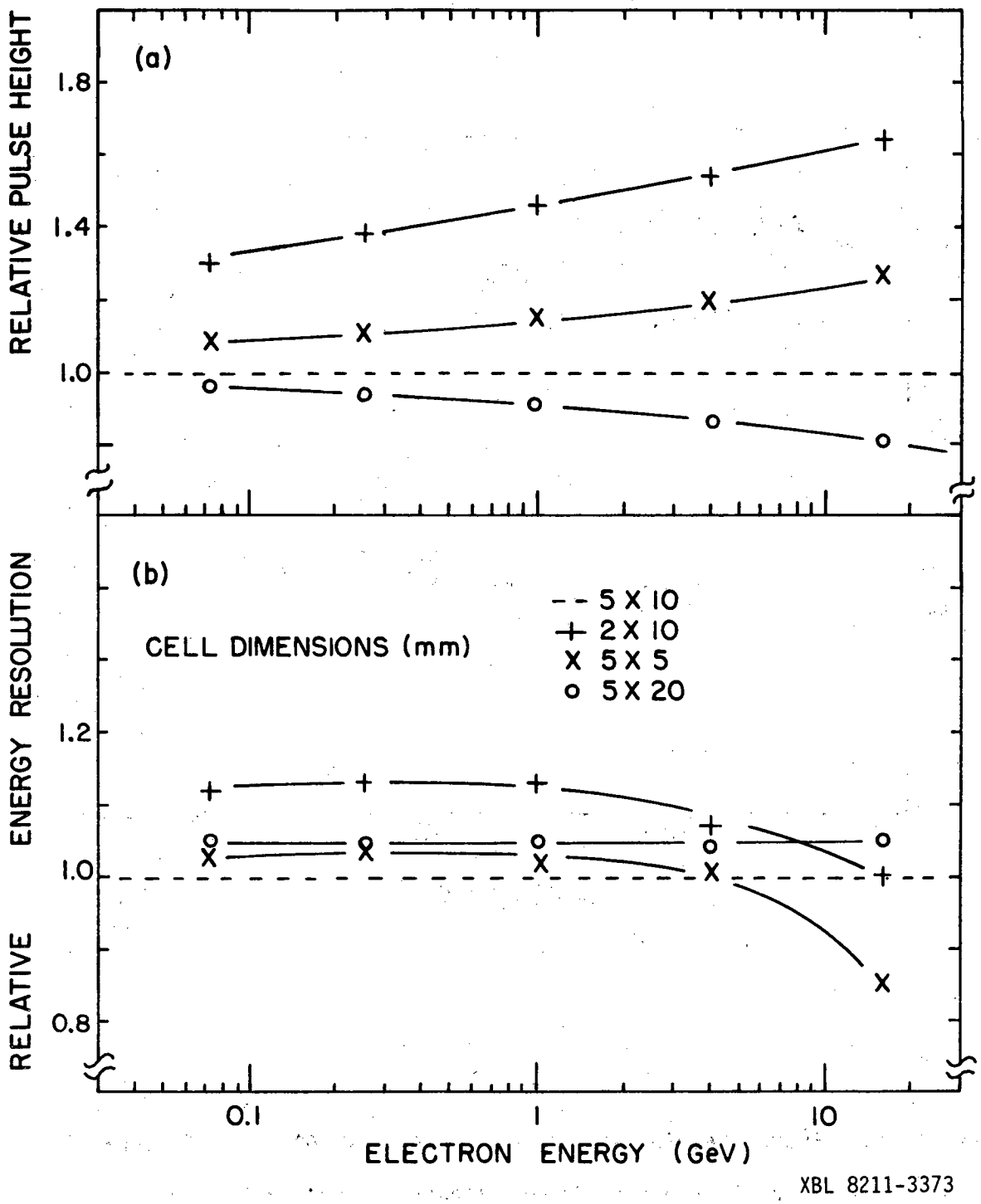

FIGURE 14. Monte Carlo simulation for various Geiger mode cell dimensions. a) Ratios of pulse heights to those for a 5 x 10 mm^2 cell. b) Ratios of energy resolutions to those for a 5 x 10 mm^2 cell.

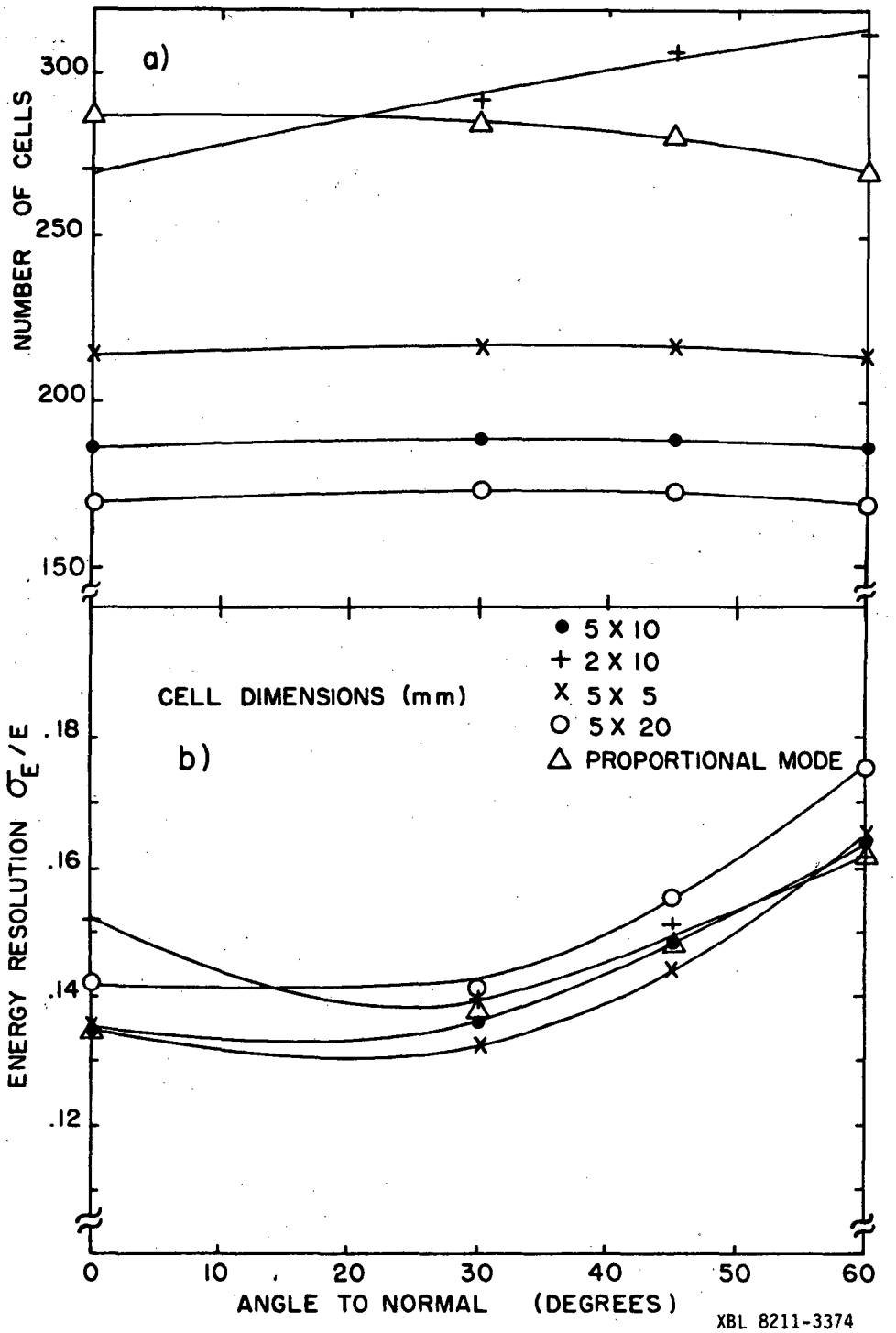

FIGURE 15. Simulated dependence on angle of incidence for Geiger mode operation with various cell dimensions. The electron energy is one GeV. a) number of cells. b) energy resolution. Proportional mode pulse height in arbitrary units and pulse height resolution are also shown.

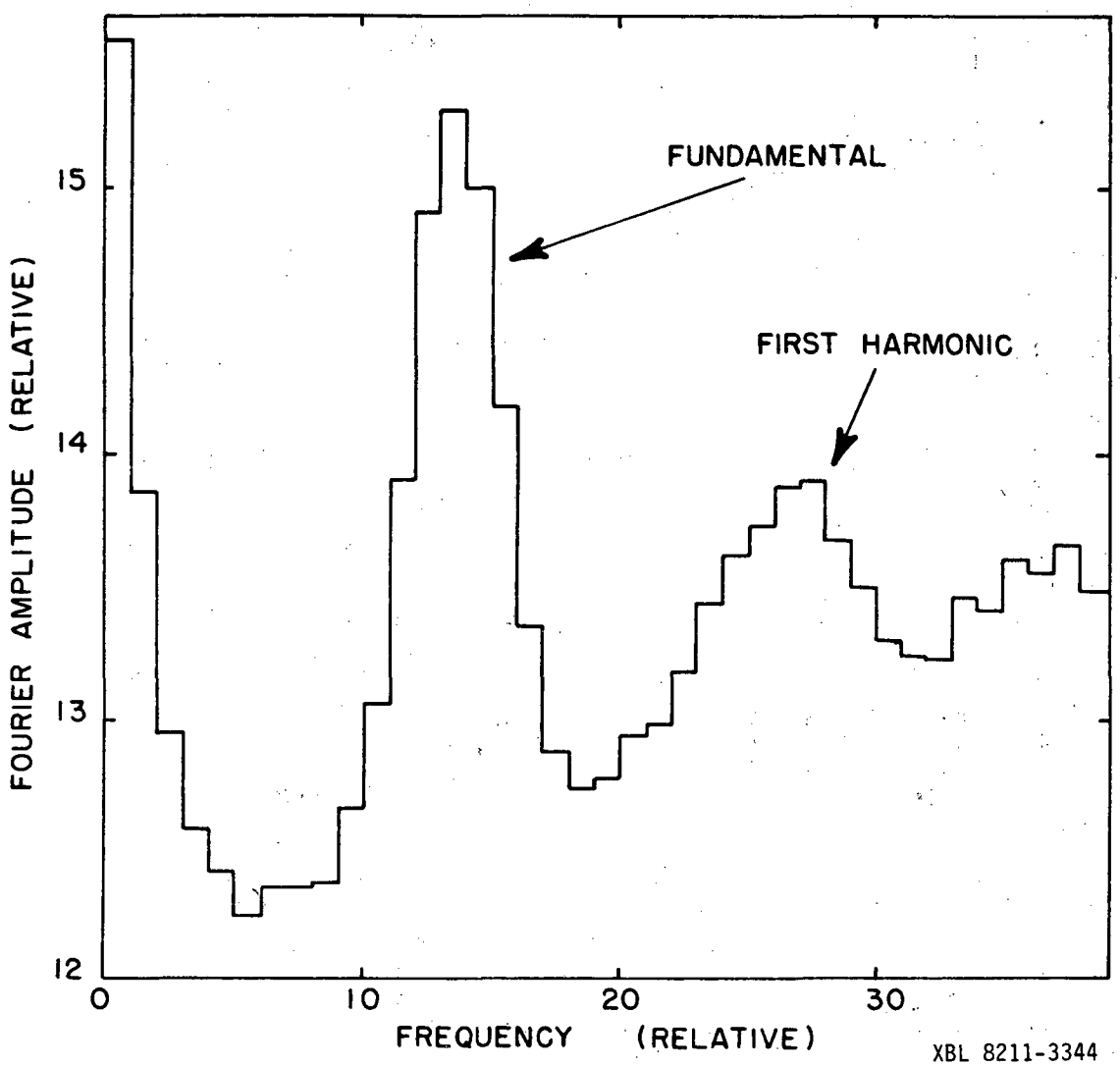

FIGURE 16. Fourier analysis of observed Geiger mode pulse height spectrum for a typical wire channel. The channel sensitivity S is obtained from the dominant peak.

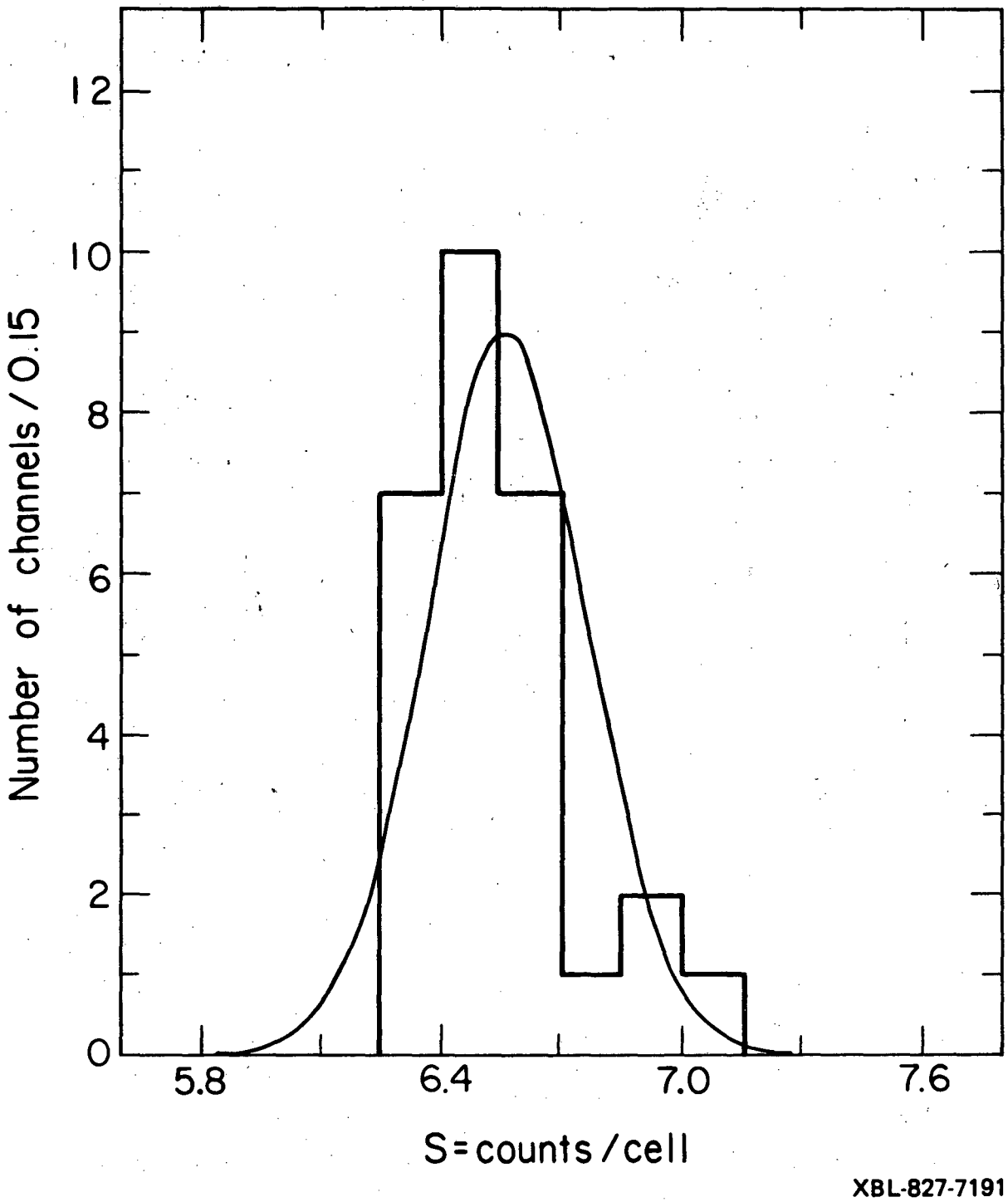

FIGURE 17. Distribution of Geiger mode counts per cell S for 28 wire channels. The fitted Gaussian is centered at S=6.56 counts/cell, with rms width σ_s=0.20 counts/cell.

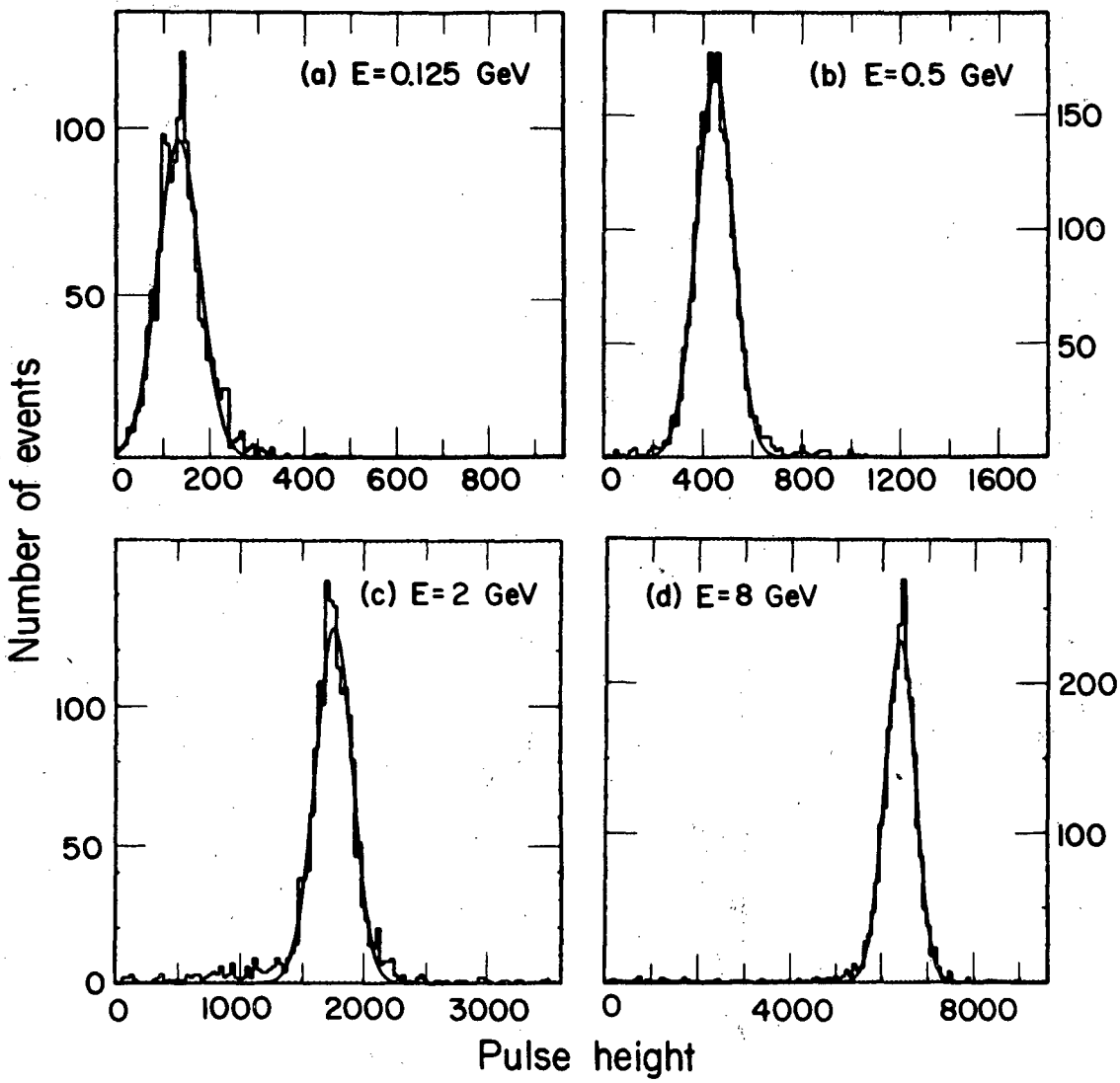

XBL 826-1532

FIGURE 18. Distributions of total Geiger mode charge for electrons at various energies. The smooth curves are Gaussian fits following the procedure described in the text.

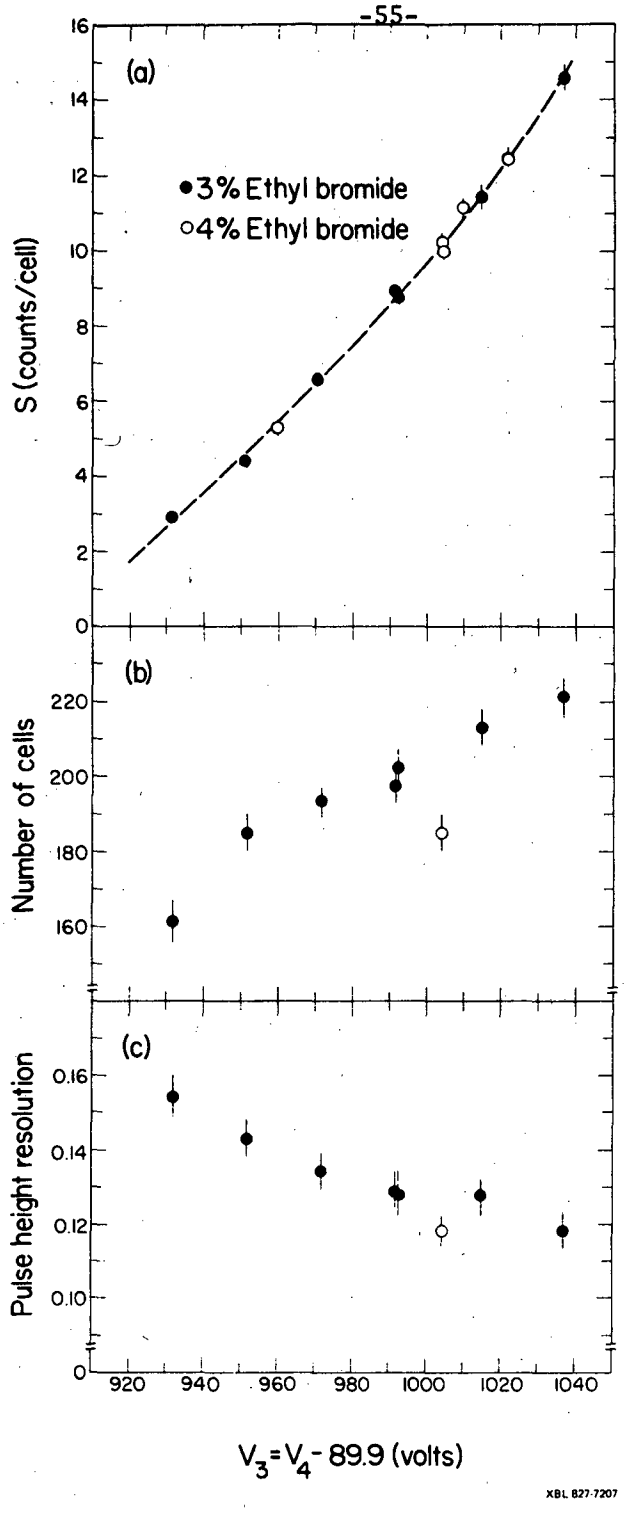

FIGURE 19. Voltage dependence of Geiger mode measurements presented in Tables I, II and III. The voltage scale for the four percent ethyl bromide data is shifted by 89.9 volts. a) Measurements of S for electrons and pions at three and four percent ethyl bromide concentration. The dashed line is the fit, $S = 0.003\ (V - 868.7)^{1.66}$ b) Total number of cells for 1 GeV electrons. c) Pulse height resolution for 1 GeV electrons.

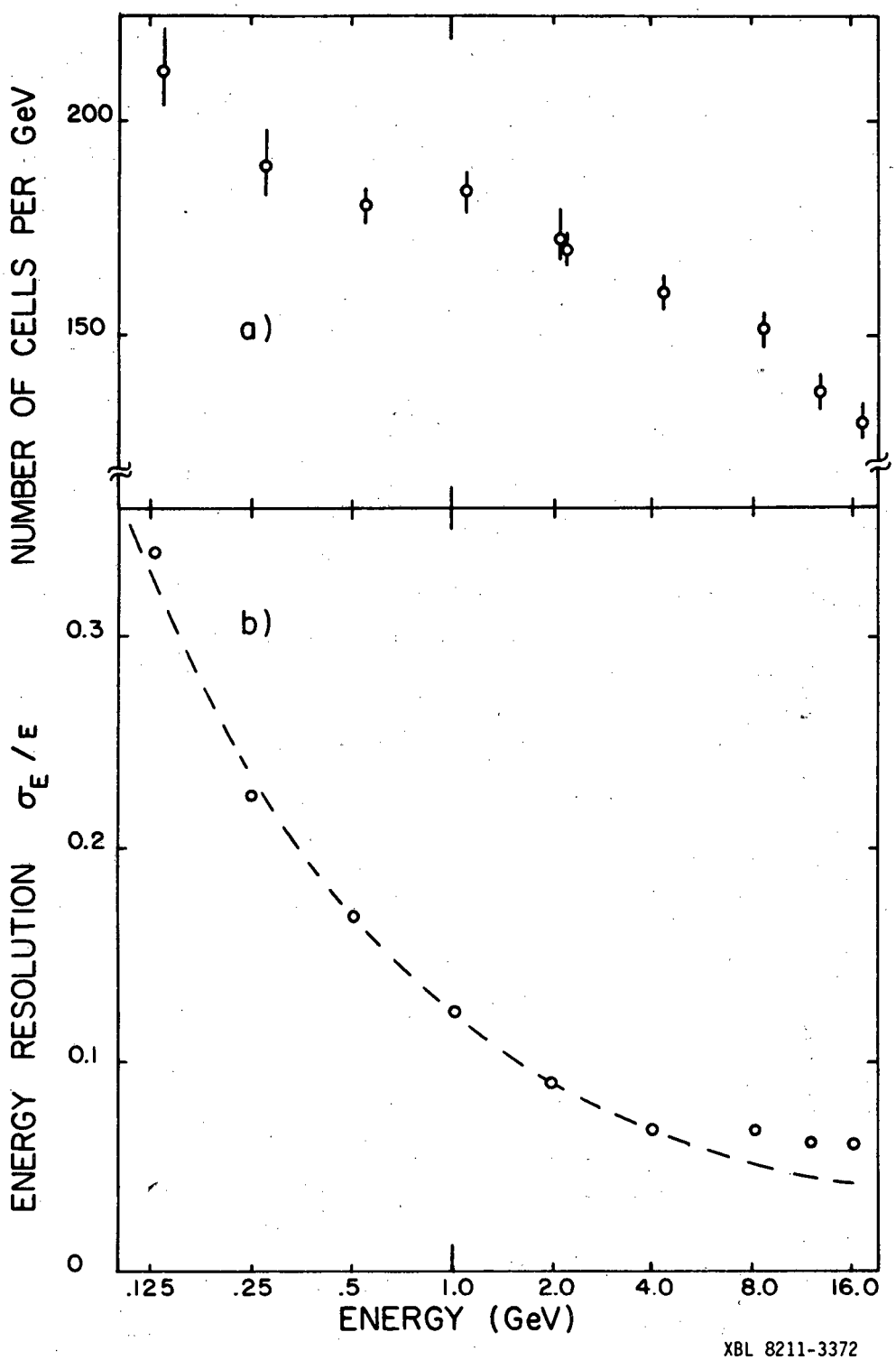

FIGURE 20. Energy dependence of Geiger mode measurements shown in Table III. a) Number of Geiger mode cells per GeV as a function of electron energy. b) Energy resolution obtained from wire signals. The dashed curve is an empirical fit, $\sigma_E/E = 0.011 + 0.112/[E(GeV)]^{\frac{1}{2}}$

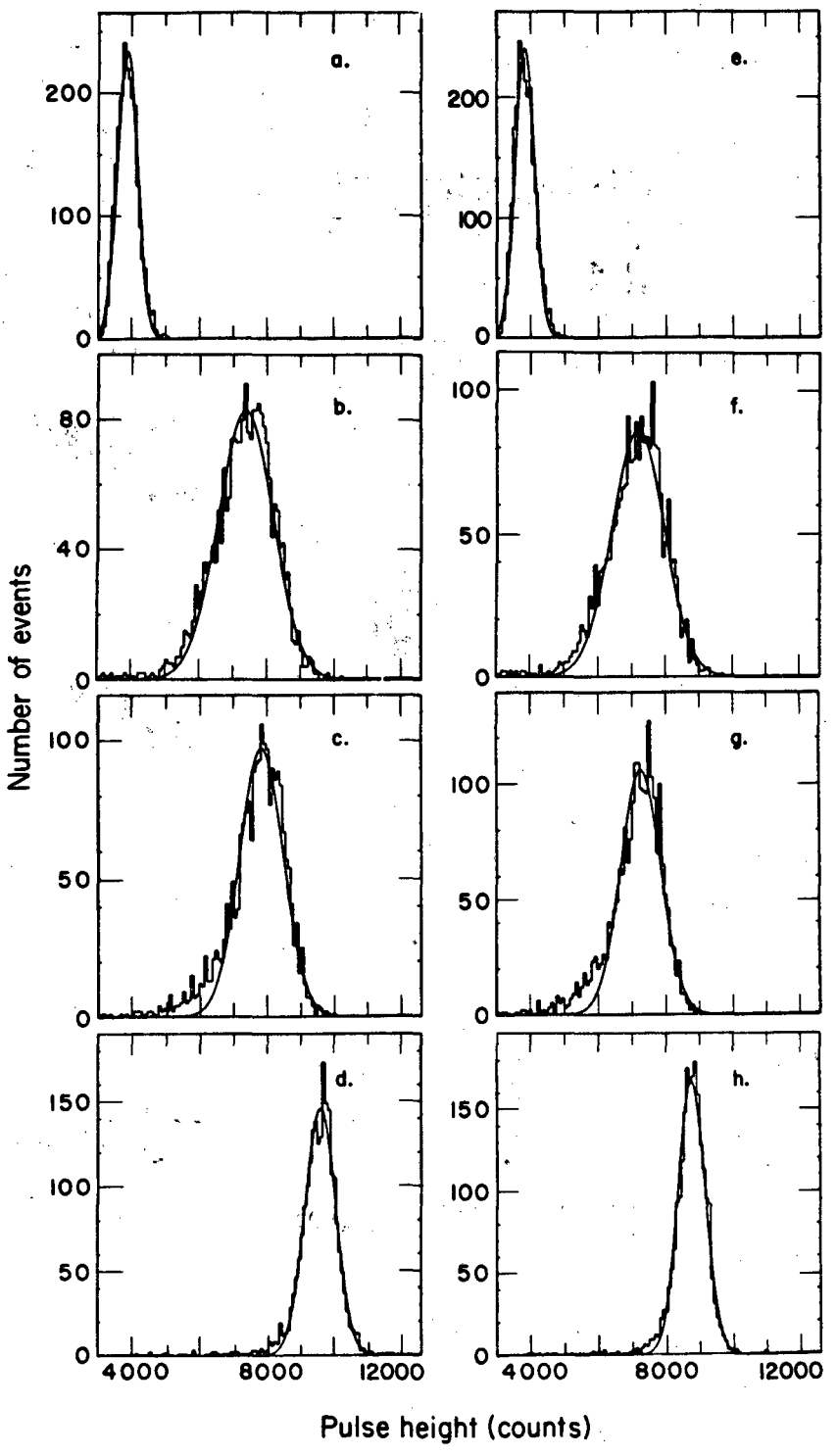

FIGURE 21. Geiger mode pulse height measurements for 12 GeV electrons for wire (a-d) and strip (e-h) channels. Pairs of distributions (a,e), (b,f), (c,g), (d,h) are for one, two, three and four submodules, respectively.

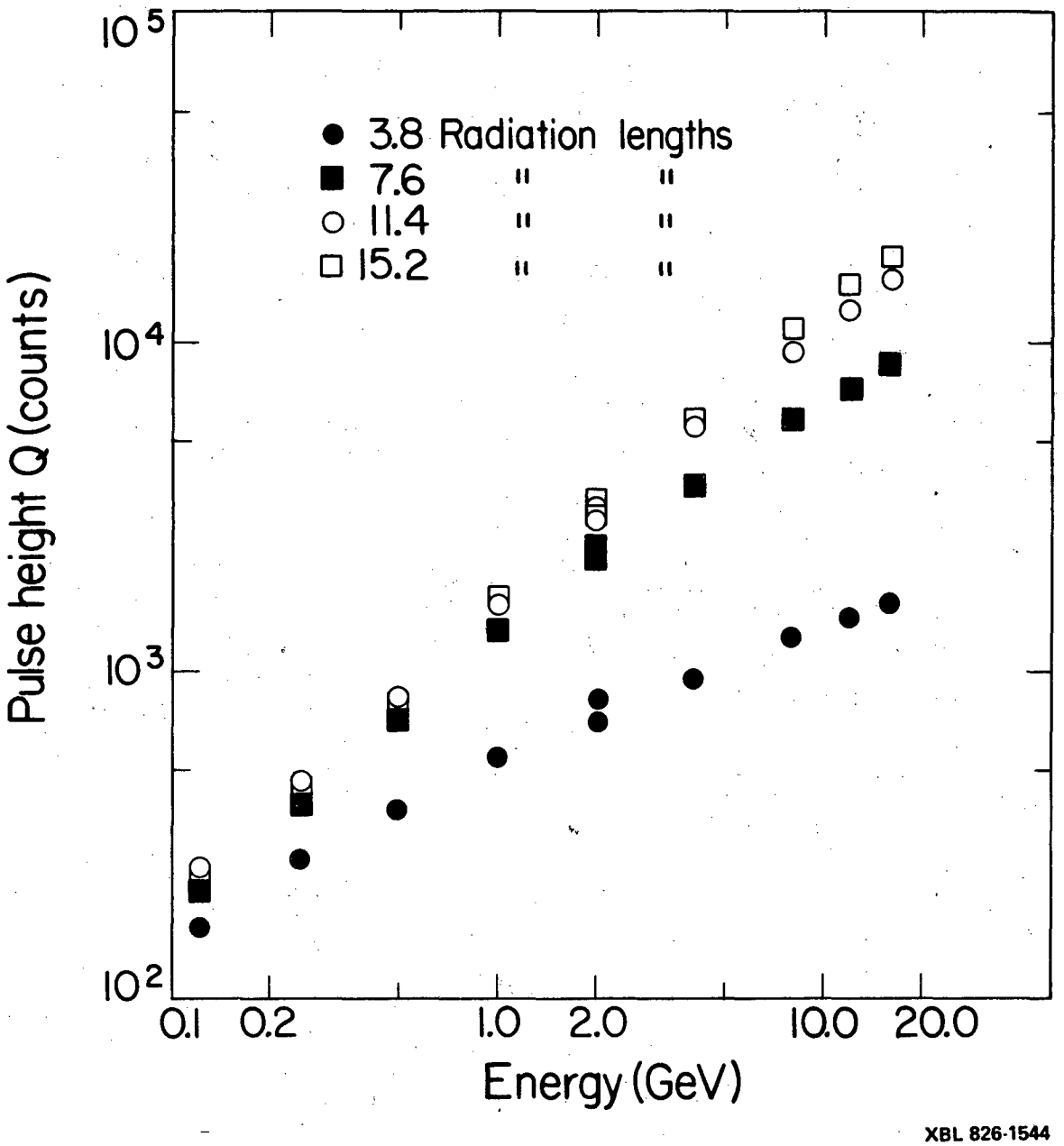

FIGURE 22. Geiger mode pulse height measurements as a function of electron energy for four calorimeter thicknesses.

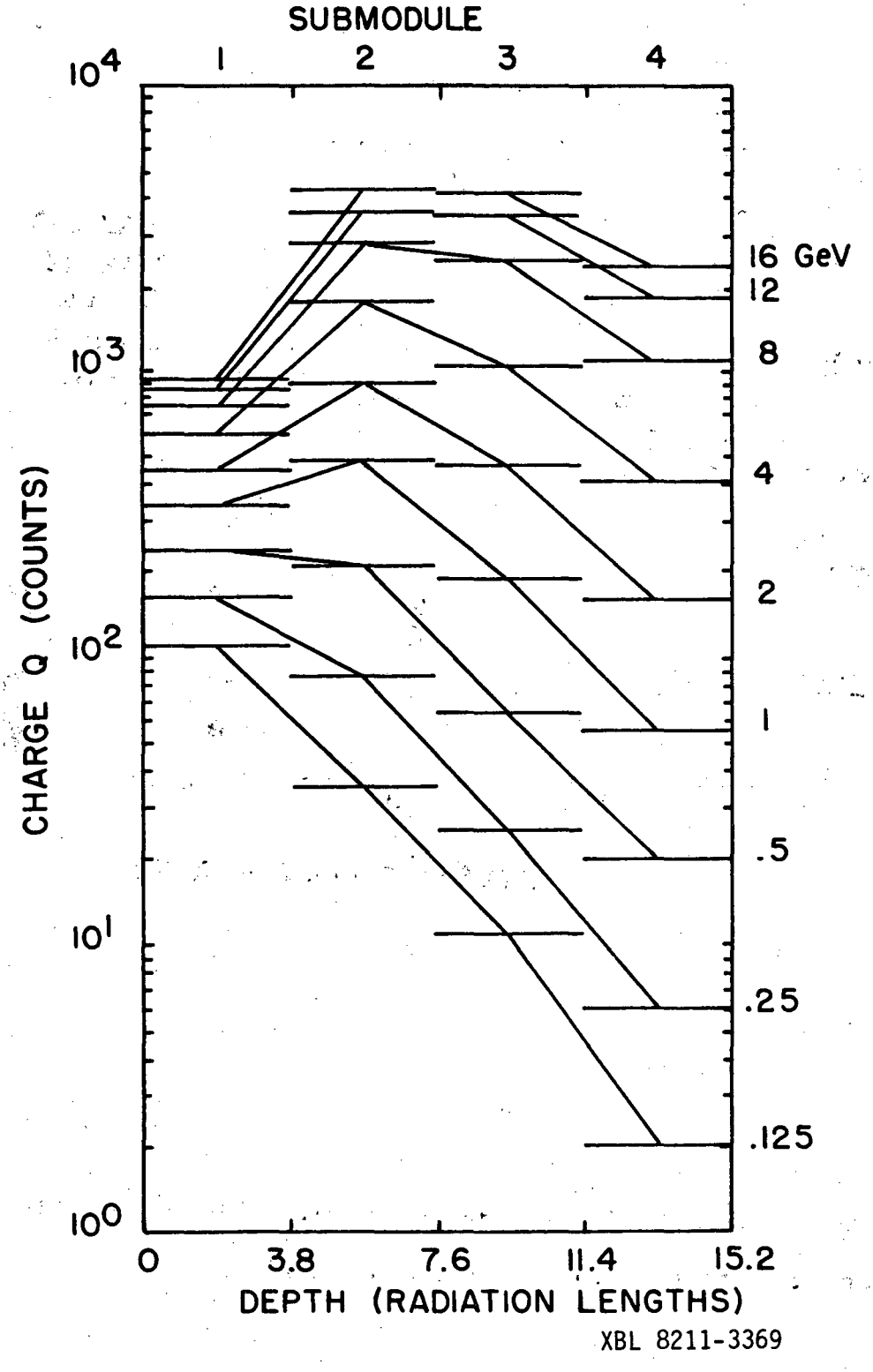

FIGURE 23. Measured Geiger mode shower development in depth for electron energies shown at right. Each horizontal line represents the signal summed over the entire submodule. See also Table IV.

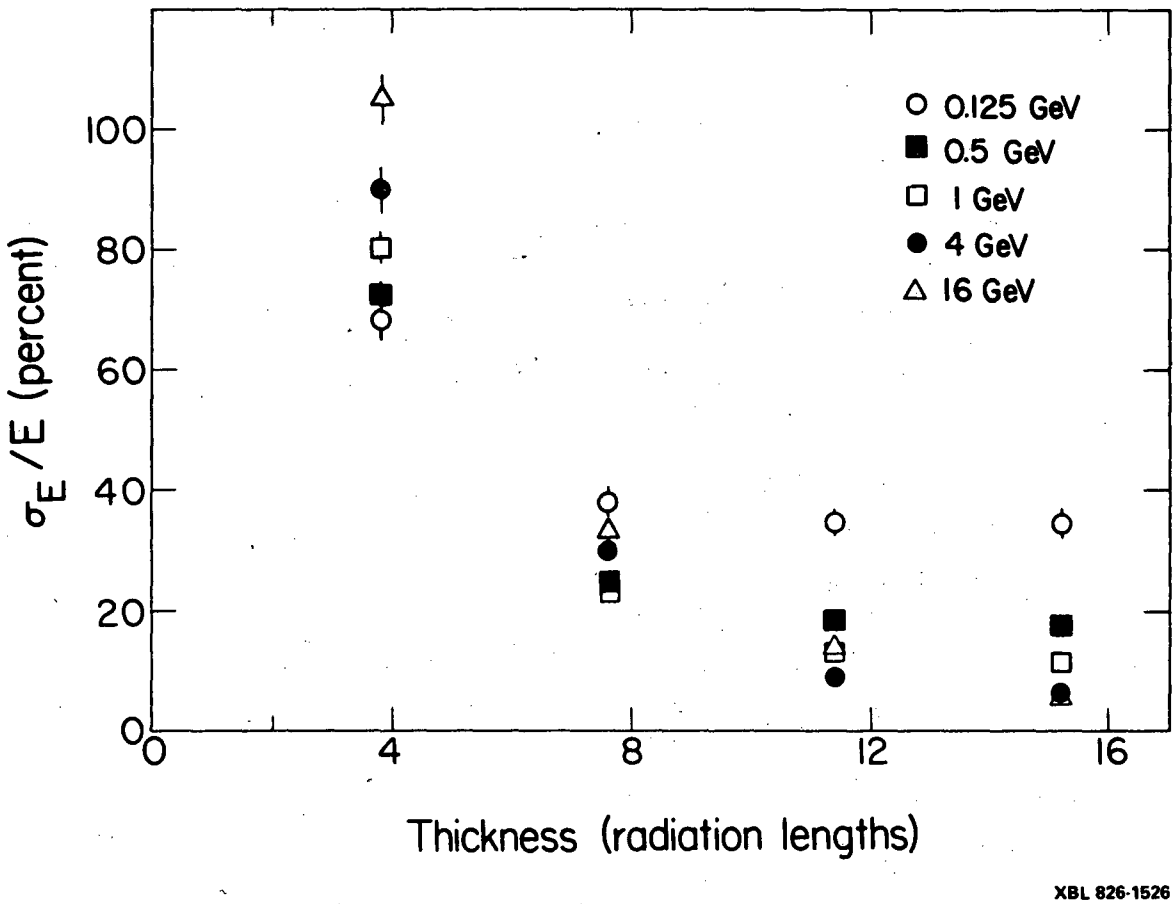

FIGURE 24. Measured Geiger mode energy resolution as a function of calorimeter thickness for five electron energies.

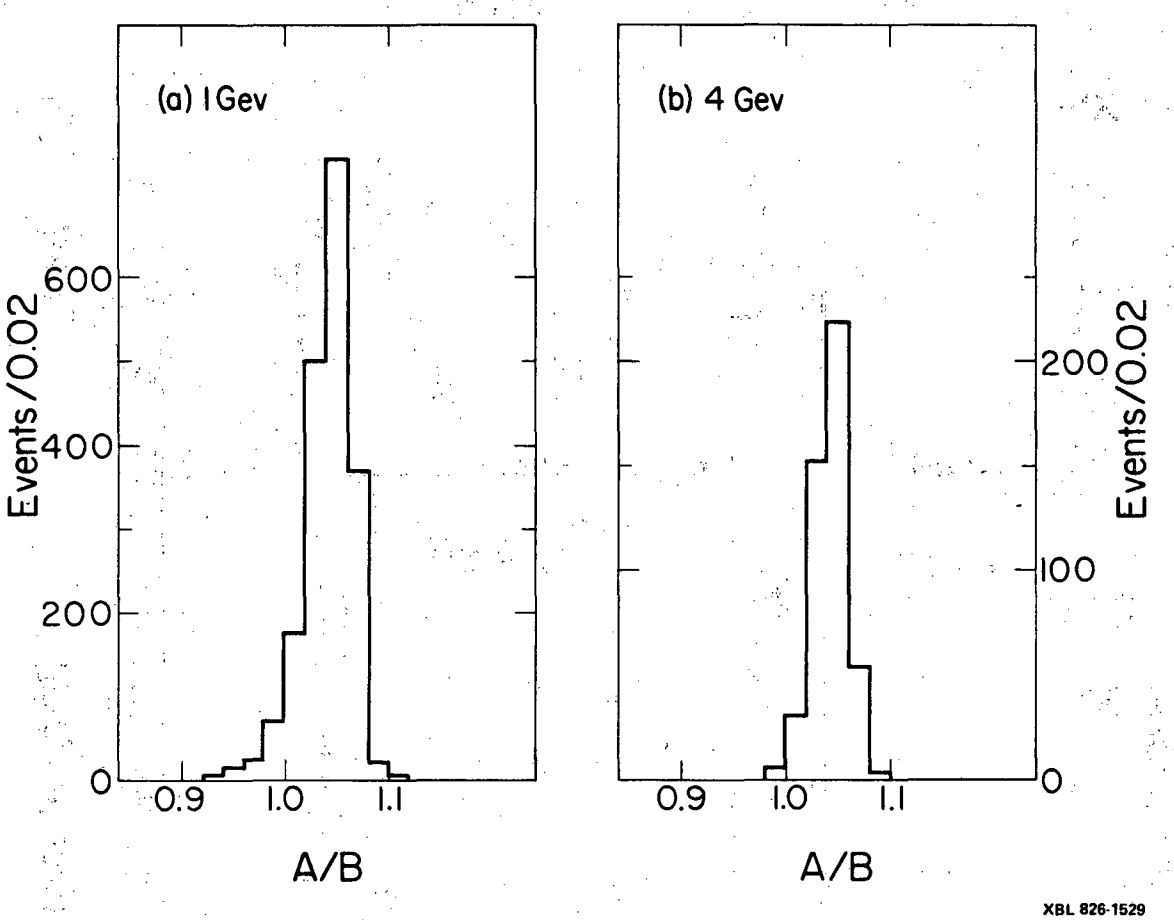

FIGURE 25. Ratio of Geiger mode strip channel signals on upstream A and downstream B cathodes of first (18 layer) submodule. Fitted parameters are given in Table V.

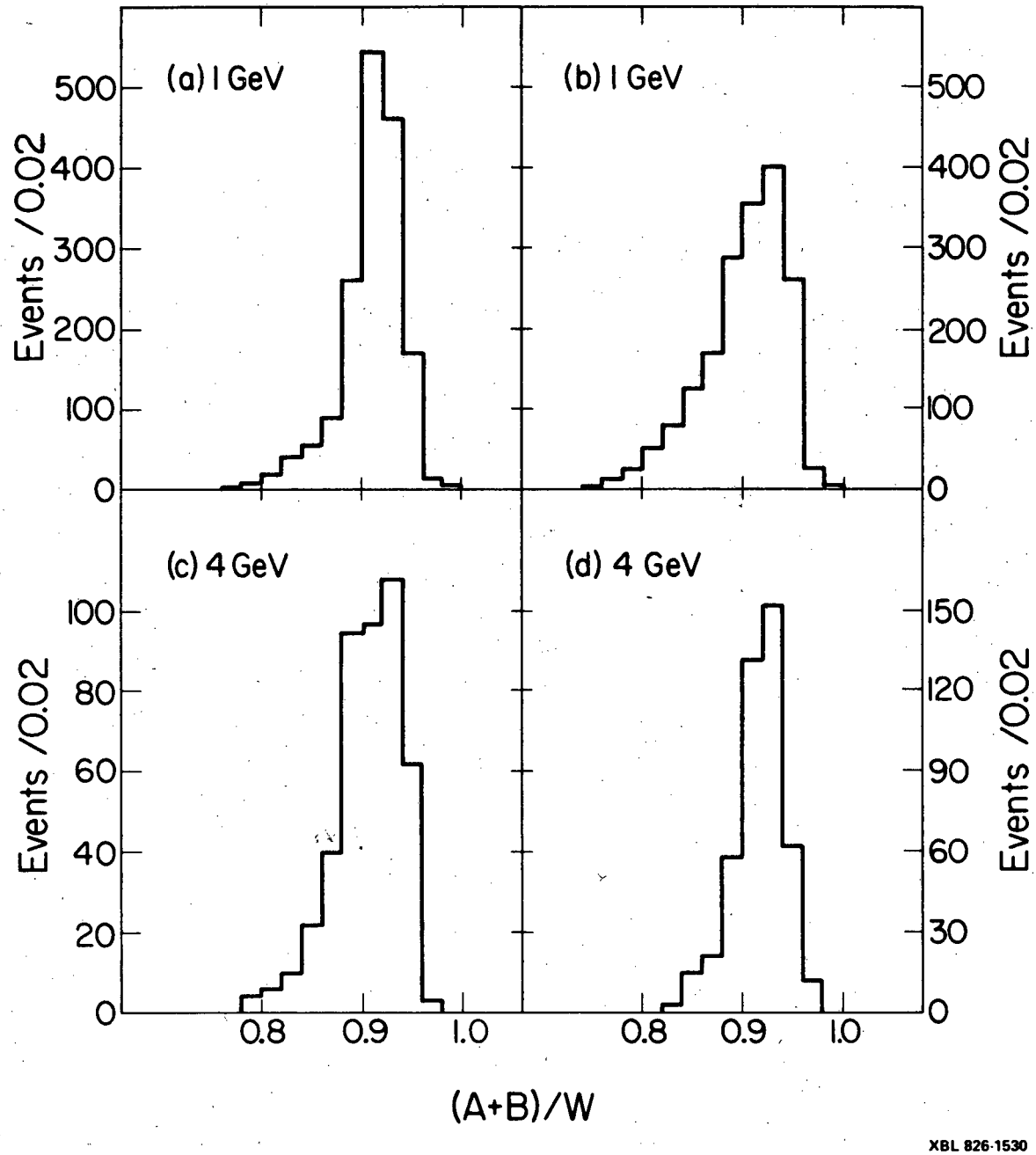

FIGURE 26. Ratio of Geiger mode strip channel (A + B) to wire channel signals in first submodule (a,c) and full calorimeter (b,d). Fitted parameters are given in Table V.

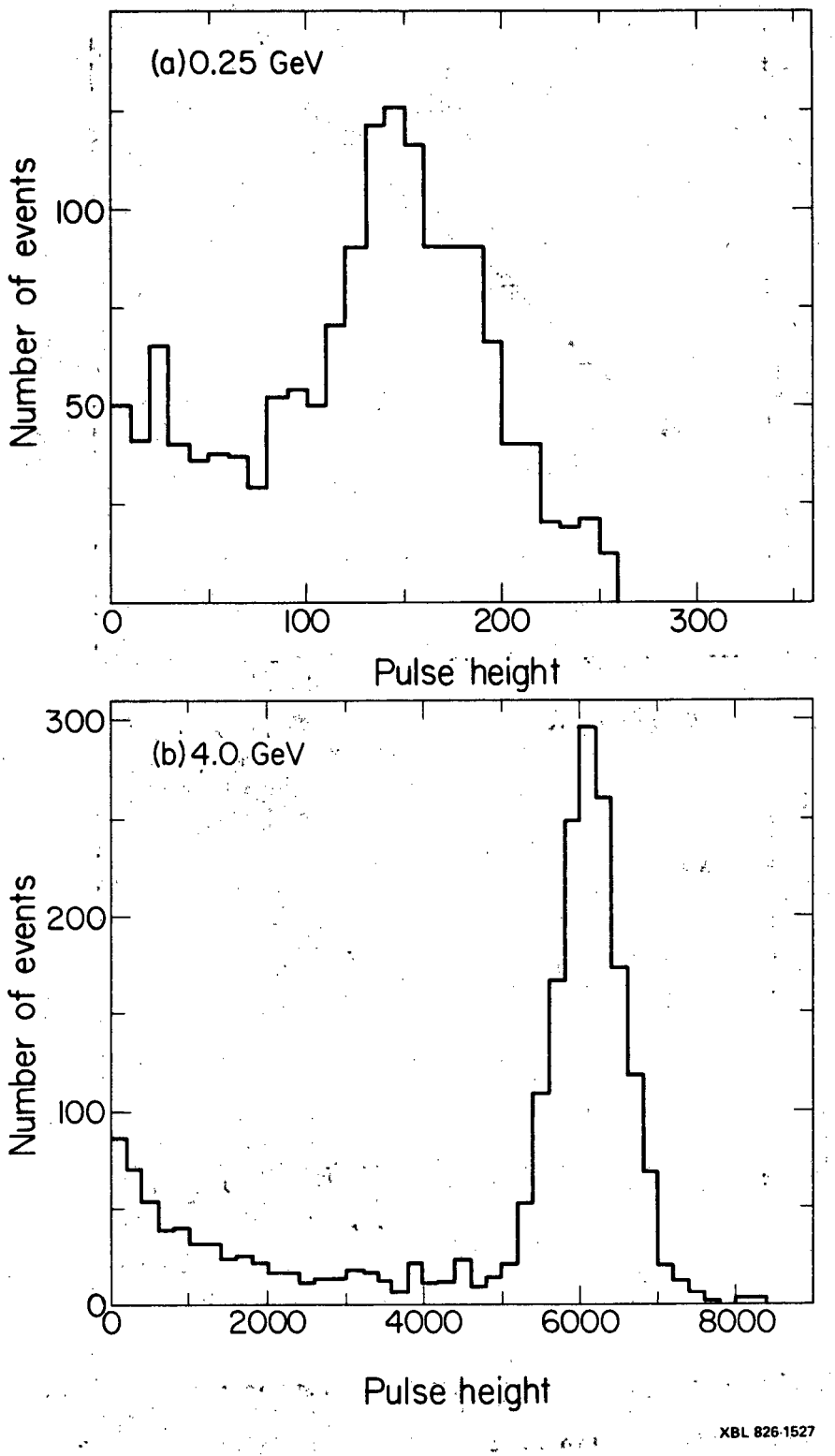

FIGURE 27. Measured pulse height spectra for electrons in proportional mode calorimeter. The data are fitted with a Gaussian plus polynomial background to extract average pulse height and width. a) 0.25 GeV. b) 4.0 GeV.

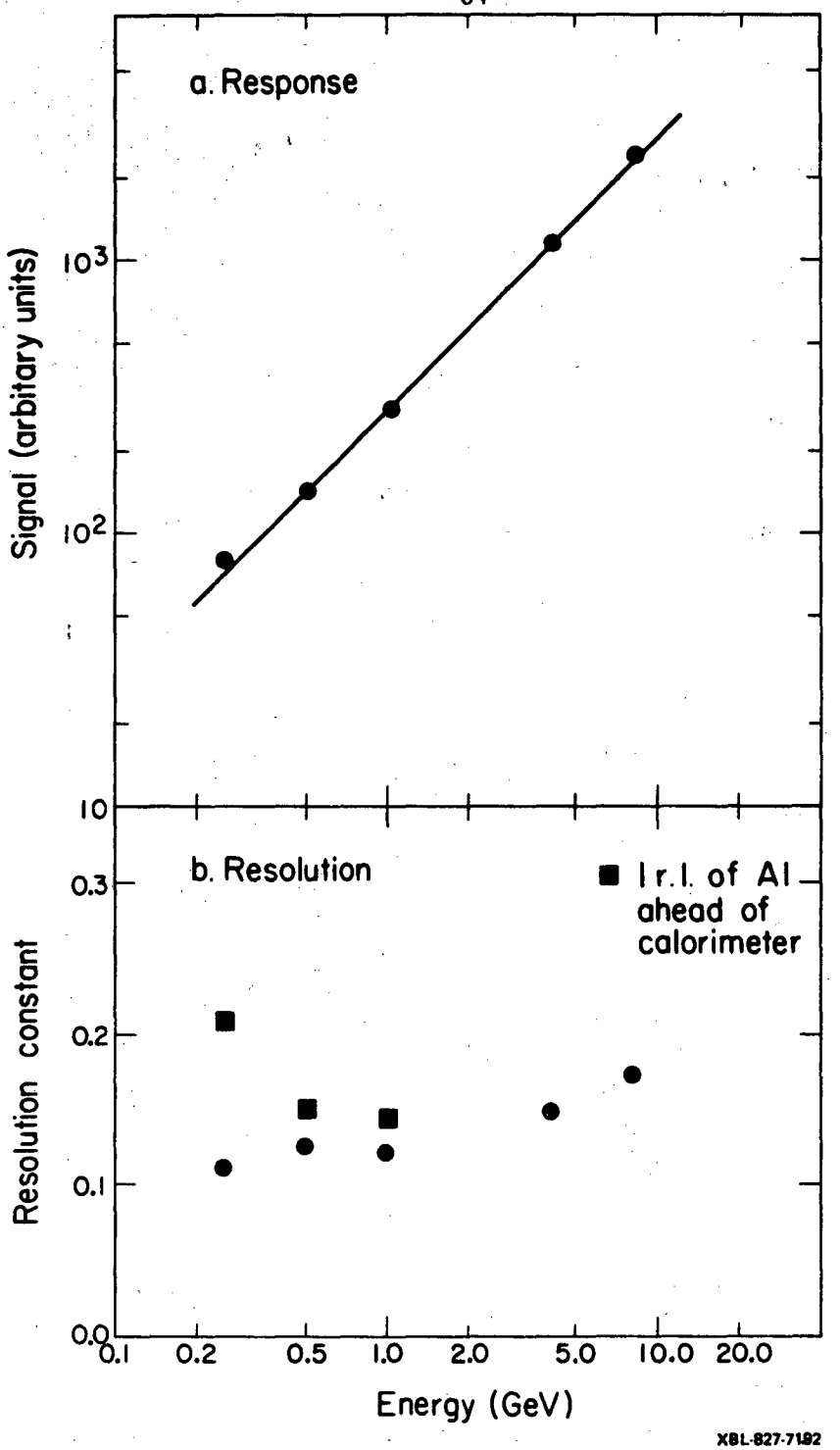

FIGURE 28. Proportional mode calorimeter measurements. a) Pulse height vs energy showing linearity of response up to 8 GeV. The straight line is drawn to guide the eye. b) Energy dependence of energy resolution. See text for definition of resolution constant α. Measurements are for 15.2 r.l. with and without a one r.l.-thick aluminum absorber ahead of the calorimeter.

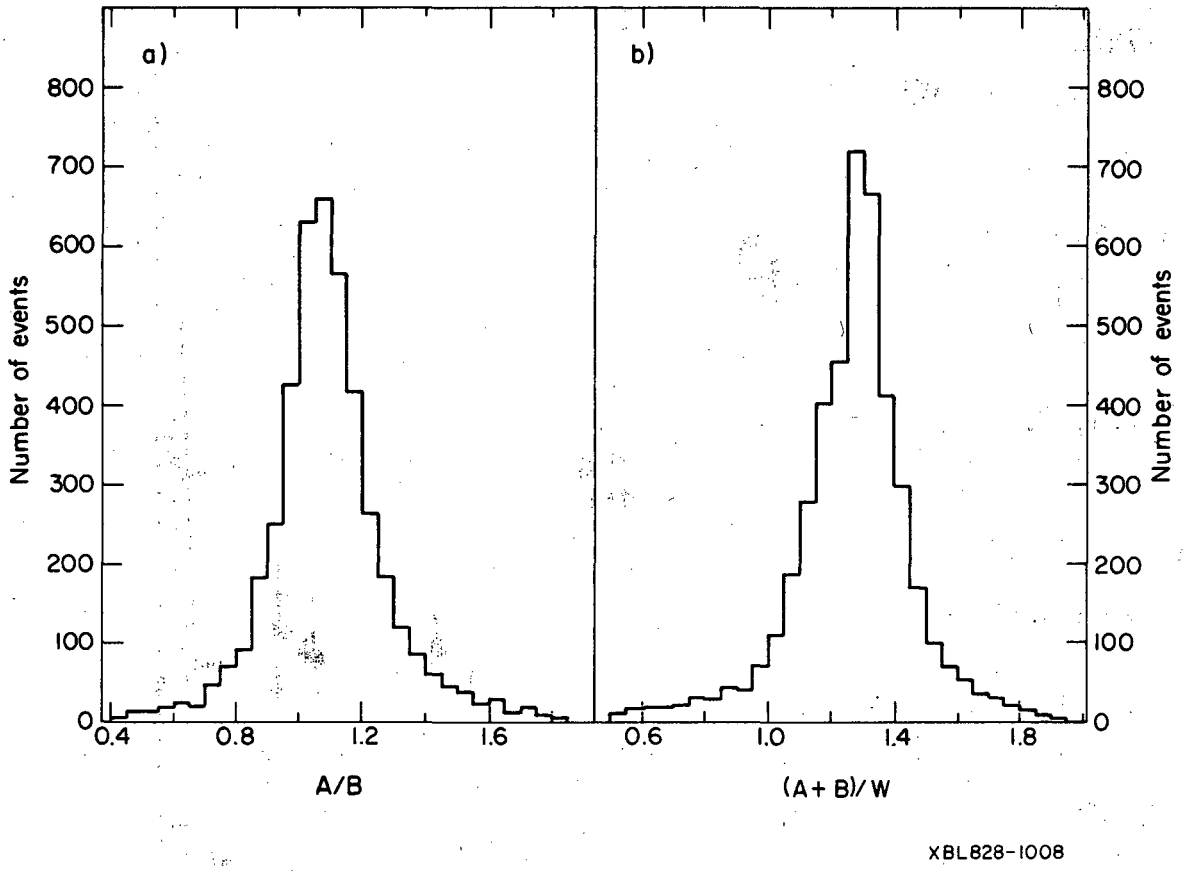

FIGURE 29. Measured charge balance in first submodule of proportional mode calorimeter for 1 GeV electrons. a) Ratio of signals on upstream A and downstream B cathode strips. b) Ratio of signals on cathode strips and sense wires.

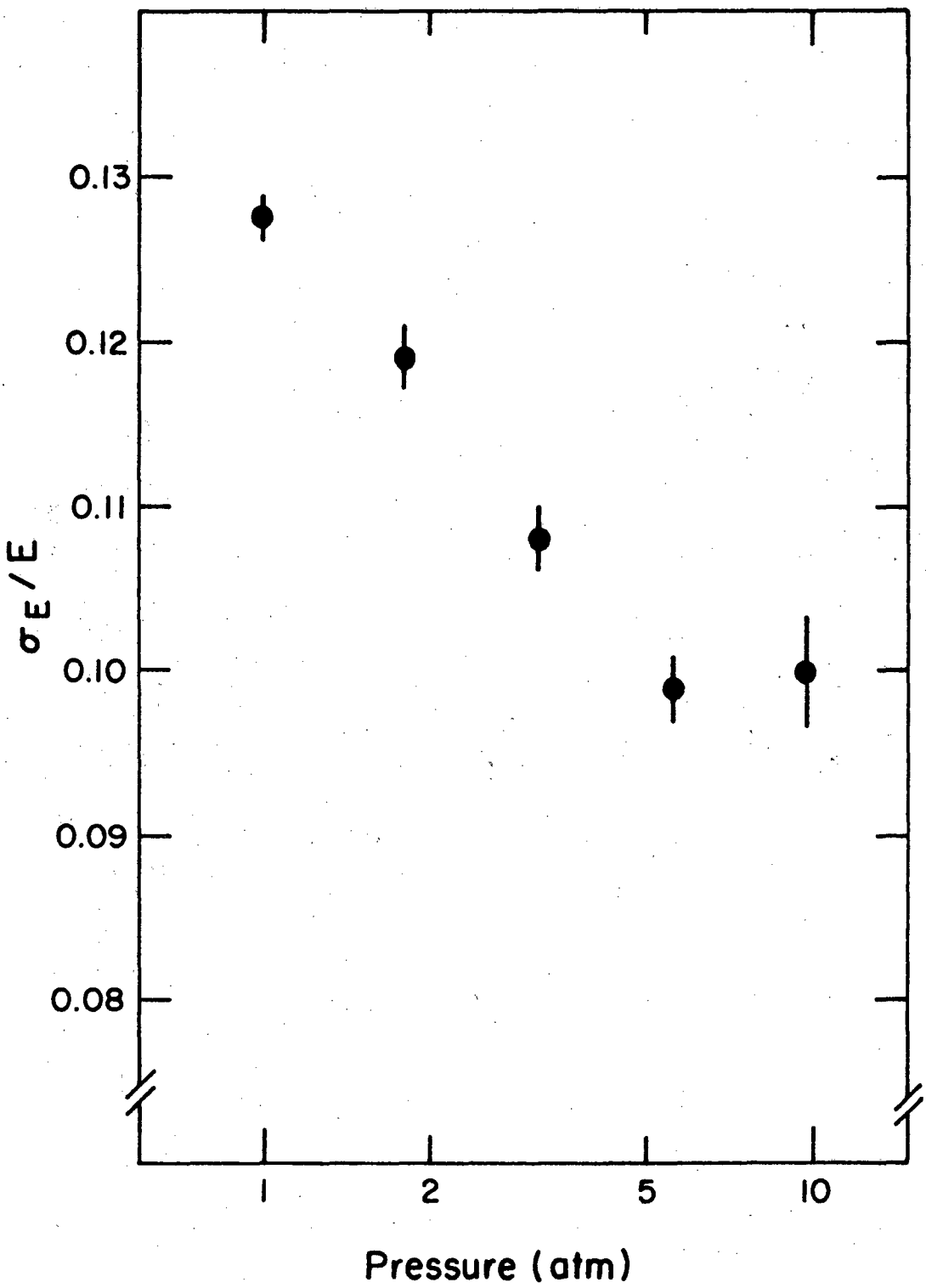

FIGURE 30. Measured pressure dependence of proportional mode energy resolution for 1 GeV electrons.

TECHNICAL INFORMATION DEPARTMENT
LAWRENCE BERKELEY LABORATORY
UNIVERSITY OF CALIFORNIA
BERKELEY, CALIFORNIA 94720